

From Easy to Hard: Progressive Active Learning Framework for Infrared Small Target Detection with Single Point Supervision

Chuang Yu^{1,2,3}, Jinmiao Zhao^{1,2,3}, Yunpeng Liu^{2,*}, Sicheng Zhao⁴, Xiangyu Yue^{5,*}

¹Key Laboratory of Opto-Electronic Information Processing, Chinese Academy of Sciences

²Shenyang Institute of Automation, Chinese Academy of Sciences

³University of Chinese Academy of Sciences ⁴Tsinghua University ⁵MMLab, The Chinese University of Hong Kong

Abstract

Recently, single-frame infrared small target (SIRST) detection with single point supervision has drawn widespread attention. However, the latest label evolution with single point supervision (LESPTS) framework suffers from instability, excessive label evolution, and difficulty in exerting embedded network performance. Therefore, we construct a **Progressive Active Learning (PAL)** framework. Specifically, inspired by organisms gradually adapting to their environment and continuously accumulating knowledge, we propose an innovative progressive active learning idea, which emphasizes that the network progressively and actively recognizes and learns more hard samples to achieve continuous performance enhancement. Based on this, on the one hand, we propose a model pre-start concept, which focuses on selecting a portion of easy samples and can help models have basic task-specific learning capabilities. On the other hand, we propose a refined dual-update strategy, which can promote reasonable learning of harder samples and continuous refinement of pseudo-labels. In addition, to alleviate the risk of excessive label evolution, a decay factor is reasonably introduced, which helps to achieve a dynamic balance between the expansion and contraction of target annotations. Extensive experiments show that convolutional neural networks (CNNs) equipped with our PAL framework have achieved state-of-the-art (SOTA) results on multiple public datasets. Furthermore, our PAL framework can build a efficient and stable bridge between full supervision and point supervision tasks. Our code are available at <https://github.com/YuChuang1205/PAL>.

1. Introduction

Single-frame infrared small target (SIRST) detection is one of the key technologies in infrared search and tracking systems [1], which has been widely used in traffic monitoring [2, 3], early warning systems [4, 5], and maritime rescue [6, 7]. However, this task faces many challenges, such as complex backgrounds, scarcity of intrinsic features and insufficient annotated data [1-3, 8-10]. Existing research mainly focuses on fully supervision, but the cost of pixel-level dense annotation is

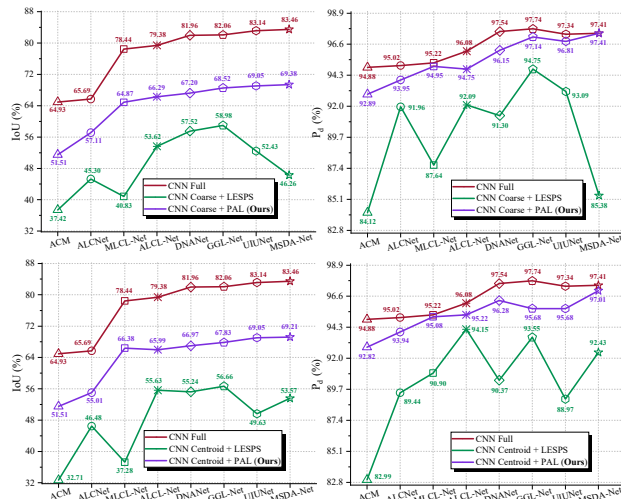


Figure 1. Comparison of different methods on the SIRST3 dataset. *CNN Full*, *CNN Coarse*, and *CNN Centroid* denote CNN-based methods under full supervision, coarse and centroid point supervision. The curve trend of CNNs equipped with the PAL framework is **basically consistent** with that of full supervision, whereas CNNs with the LESPTS framework [1] is not. In addition, compared with the LESPTS, using our PAL framework can improve by **8.53%-29.1%** and **1.07%-12.03%** in the IoU and P_d .

prohibitive. Therefore, achieving high-performance SIRST detection with single point supervision is both challenging and significant.

Early SIRST detection focus on model-driven methods [11-24]. However, these methods are often based on static background or saliency assumptions, which are easily affected by hyperparameters and lead to unstable detection performance. Compared with model-driven methods, CNNs are data-driven and can automatically learn the nonlinear relationship between input images and true labels [25]. Different from general targets, infrared small targets are small in size and lack of intrinsic features. It is difficult to achieve satisfactory detection results [1] by directly using existing general target detection methods such as the YOLO series [26-28] and SSD [29]. Therefore, existing methods focus on building proprietary SIRST detection networks by leveraging domain knowledge [2, 8-10, 30, 31]. However, existing SIRST detection methods

focus on full supervision, which requires expensive pixel-level dense annotations. To reduce the annotation cost, Ying et al. recently propose a LESPS framework that combines the existing excellent SIRST detection network with continuous pseudo-label self-evolution to achieve SIRST detection with single point supervision. However, this framework has problems such as instability, excessive label evolution, and difficulty in exerting embedded network performance.

To solve these problems, we attempt to build a new, efficient and stable SIRST detection framework for single point supervision. Inspired by organisms gradually adapting to their environment and continuously accumulating knowledge, we came up with an idea: ***The learning of network models should also be from easy to hard?*** We consider that an excellent learning process should be from easy to hard and take into account the learning ability of the current learner (model) rather than directly treating all tasks (samples) equally. On this basis, we propose an innovative progressive active learning idea, which emphasizes that the network progressively and actively recognizes and learns more hard samples to achieve continuous performance enhancement. **First**, to enable the network model to have basic task-specific learning capabilities in the initial training phase, we propose a model pre-start concept. Different from the existing methods that directly use all point labels, it focuses on selecting a portion of easy samples that can generate relatively fine pseudo-labels and put them into the training pool for initial fully supervised training. For this task, an easy-sample pseudo-label generation (EPG) strategy is constructed to achieve the selection of easy samples. **Second**, considering that the pre-started model has the ability to recognize some hard samples and the pseudo-labels entering the training pool are not refined, we construct a fine dual-update strategy that includes coarse outer updates and fine inner updates. Unlike the existing methods that perform only label self-evolution, the fine dual-update strategy not only selects "easy samples" within the current model's cognitive ability from hard samples into the training pool, but also performs fine label updates on samples that have entered the training pool. The fine dual-update strategy is periodically used, which alternately promotes model performance improvement and harder sample learning. **Finally**, we observe an interesting phenomenon: the existing framework has the problem that the evolution area does not shrink after expansion. To solve this problem, a decay factor is rationally introduced to achieve a dynamic balance between the expansion and contraction of target annotations.

In summary, we construct a PAL framework for SIRST detection with single point supervision that focuses on learning from easy samples to hard samples. From Fig. 1, it achieves significant performance improvements and can build an efficient and stable bridge between SIRST

detection with full supervision and single point supervision. The contributions can be summarized as follows:

1. Inspired by organisms gradually adapting to the environment and continuously accumulating knowledge, we first propose an innovative progressive active learning idea, which emphasizes that the network progressively and actively recognizes and learns more hard samples to achieve continuous performance enhancement.

2. A model pre-start concept is proposed, which focuses on selecting a portion of easy samples and can help models have basic task-specific learning capabilities. For this task, we construct an easy-sample pseudo-label generation strategy to achieve the selection of easy samples.

3. A fine dual-update strategy is proposed, which can promote reasonable learning of harder samples and continuous refinement of pseudo-labels.

4. To alleviate the risk of excessive label evolution, a decay factor is reasonably introduced, which helps achieve a dynamic balance between the expansion and contraction of target annotations.

2. Related Work

SIRST detection can be divided into model-driven non-deep learning methods [11-24] and data-driven deep learning methods [2, 3, 8-10, 30, 31-33]. Early research focus on model-driven methods, including background suppression-based methods [11-15], human visual system-based methods [16-20], and image data structure-based methods [21-24]. The above methods perform well in specific scenarios but require careful model design and hyperparameter tuning. Subsequently, data-driven deep learning methods gradually replaced model-driven methods. In the early days, Dai et al. propose an asymmetric context module [32] and further introduce a local contrast metric to improve detection performance [30]. Subsequent research focuses on the utilization of domain knowledge [2, 8-10, 31] and the improvement of network structure [3, 33]. The above methods achieve excellent performance in the SIRST detection with full supervision. However, pixel-wise dense annotations are very expensive, which motivates us to exploit the more cost-effective point-level weak supervision [34].

Point-based supervision is of great significance and has been widely studied in object detection [35-37], object counting [38-40], and semantic segmentation [34, 41-49]. We focus mainly on image segmentation in this paper. For weakly-supervised semantic segmentation with point labels, existing methods focus on general object segmentation [34, 41, 42] and panoptic segmentation [43-45]. However, the above studies mainly focus on segmenting general targets with rich colors, fine textures, and even require multiple annotation points. Considering the characteristics of this task, directly using the above methods will fail. To solve this problem, Ying et al.

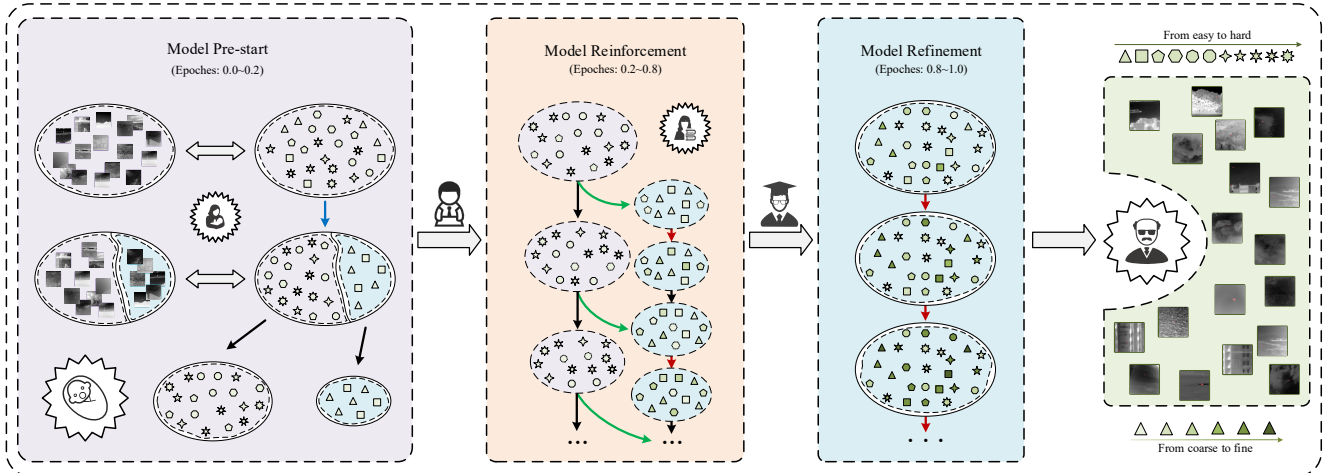


Figure 2. The PAL framework. The purple ellipse area is the preparation pool, which contains samples that the current model cannot recognize and train. The blue ellipse area is the training pool, which contains samples that the current model can train. Each shape refers to a different level of difficulty, and the color depth refers to the refinement of the corresponding pseudo-label. The blue arrow denotes the easy-sample pseudo-label generation strategy. The green arrows and red arrows denote the coarse outer updates and fine inner updates.

propose a LESPS framework [1], which uses the intermediate network predictions during the training phase to update the current label and serve as supervision. However, the LESPS framework suffers from instability, excessive label evolution, and difficulty in exerting embedded network performance. Therefore, we attempt to construct a new, efficient and stable framework.

3. The Proposed Model

3.1. Overview

To achieve fine SIRST detection with single point supervision, we construct an end-to-end PAL framework. From Fig. 2, the proposed training framework can be mainly divided into three phases: model pre-start, model enhancement, and model refinement. The model pre-start phase aims to give model the initial ability. Specifically, an EPG strategy is constructed to divide all training samples into two groups: easy samples and hard samples. The selected easy samples are transferred to the training pool and trained with full supervision in the initial stage. For details, see Section 3.3. Subsequently, the model will enter the model enhancement phase. Based on the cognitive and learning capabilities of the current model, we use it to detect the remaining hard samples to select "easy samples" that meet the selection rules. The "easy samples" will be transferred to the training pool for training to enable the model to learn more hard samples. For details, see Section 3.4. In this phase, we will periodically assess the remaining hard samples in the preparation pool. In addition, the pseudo-labels of samples entering the training pool during the model pre-start phase and model enhancement phase are to be refined. Therefore, we periodically apply the proposed fine inner updates in the model enhancement

phase and the model refinement phase to gradually generate more refined pseudo-labels.

3.2. Progressive Active Learning

We consider that an excellent learning process should be from easy to hard and take into account the learning ability of the current learner (model) rather than directly treating all tasks (samples) equally. Therefore, a progressive active learning idea is proposed for the first time. From Fig. 3, for an initial model, it is like a newborn baby. Despite its unlimited potential, its currently accepted knowledge is limited and should be simple. At this time, a mother's role plays an important role. She will not immediately try to teach the baby the principles of quantum mechanics, but will consciously impart to the baby some simple language expression and logical thinking skills. Based on this, we propose a pre-start concept. The easy samples are selected for initial fully supervised training. The model will have basic task-specific learning capabilities through this phase, just like the student model in Fig. 3.

For students, they will come up with ideas for their future careers and work towards them. With basic skills, they can assess the difficulty of the tasks they face and learn from easy to hard, thereby continuously enhancing their abilities. Based on this, we use the pre-started model to test the hard samples to determine the samples that can be learned. With the addition of hard samples, the network will strengthen its cognitive and learning ability of hard samples and will not catastrophically forget easy samples. Therefore, by setting the execution cycle, the network can progressively and actively recognize and learn more hard samples. Considering that CNNs require many sample, given labeled training samples are valuable. However, simply relying on the continuous active learning may result

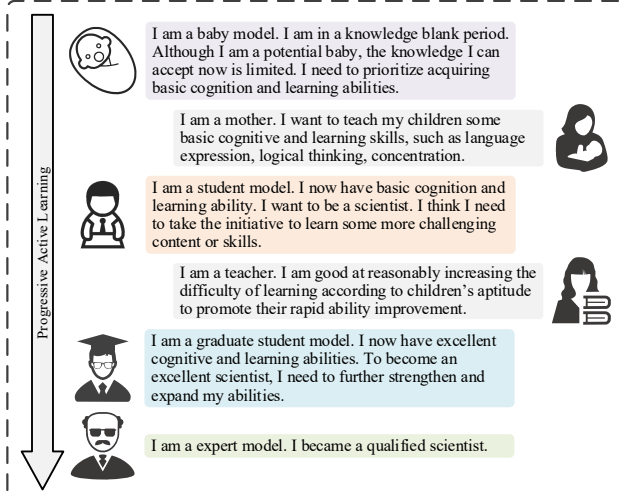


Figure 3. Schematic representation of progressive active learning.

in some hard samples never entering the training pool, causing the model to fail in some difficult scenarios.

Therefore, inspired by the guiding role of teachers in the growth of students' learning ability, we further introduce additional beyond-expectation guidance. According to students' progress, teachers can appropriately increase the difficulty of tasks to promote the rapid improvement of students' abilities and the timely completion of the learning content. Based on this, we increase the difficulty of the samples entering the network based on its current capabilities, thereby stimulating the model's learning potential and ensuring that all samples can eventually enter the training pool. At this time, the generated model is like the graduate student model in Fig. 3, which has excellent abilities and has learned the necessary knowledge.

However, to eventually become a scientist, one needs to refine all knowledge based on existing abilities to reach the expert stage where one can apply it proficiently. Based on this, we divide a model refinement phase to allow the network to learn all samples. In this phase, we periodically apply the proposed fine inner updates to promote model refinement learning.

3.3. Model pre-start

We consider that compared with directly using point labels for training, if we can select a part or even a small number of easy samples that can generate relatively fine pseudo-labels for initial full-supervised training, it will help the network to have basic SIRST detection capabilities. Therefore, different from existing methods [1, 50], we propose a model pre-start concept. Considering the detection scene, imaging characteristics and target properties, infrared small targets are characterized by small size, high brightness and a lack of strong semantic contextual relationships with the surrounding environment [3, 9, 30, 31]. Some target areas can be detected by

model-driven methods. However, they are often not robust and prone to false detections [31]. Therefore, we propose an EPG strategy to achieve the selection of easy samples, as shown in Fig. 4.

We consider that processing the local image patch where the target area is located instead of the entire image can effectively reduce the interference of complex backgrounds. Therefore, we use the given point label as the center point to obtain the local image patch with the target. To effectively and precisely detect the target area in the image patch, we first use the Gaussian filtering to appropriately suppress the noise in the image. Second, the Canny operator [51] is used to obtain the contour of the target area. Finally, we use a morphological closing operation to reduce the broken phenomenon of the extracted contour and fill the area enclosed by the contour to obtain the segmentation result of the image patch.

To select easy samples and refine the corresponding pseudo-labels, we make full use of the given point labels and the segmentation results. **First**, we use the given point label to assess the connected area in the segmentation result. For the connected area that are hit by the label point and whose area is smaller than the set threshold, it is identified as the true target area. Other connected areas that do not meet the conditions are considered as false detection areas, which are removed. **Second**, we calculate the target-level recall rate. If it is greater than and equal to the set threshold, it is regarded as an easy sample. The threshold is set to 0.8. Otherwise, it is a hard sample. **Third**, each segmented image patch of the easy sample is added to a pure black background with the original image size to generate a pseudo-label. **Finally**, the given point labels are added to the pseudo-labels to annotate the missed targets and generate relatively fine pseudo-labels.

Through the proposed EPG strategy, a portion of easy samples are selected for initial fully supervised training. The model pre-start phase can help models have basic task-specific learning capabilities. It also avoids hard samples from introducing too much noise or misleading information in the early phase of network training.

3.4. Fine dual-update strategy

The quality of pseudo-labels directly affects the performance of the final generated model. Different from existing frameworks that directly use label self-evolution to iteratively evolve all point labels [1, 50], we propose a fine dual-update strategy. This strategy includes coarse outer updates and fine inner updates.

1) Coarse outer updates (COU): After the model pre-start phase, the model has basic SIRST detection capabilities. Based on it, we detect the remaining hard samples to select "easy samples" that meet the selection rules into the training pool. The COU can be divided into three steps: determining recognizable samples, eliminating false targets, and supplementing missed targets.

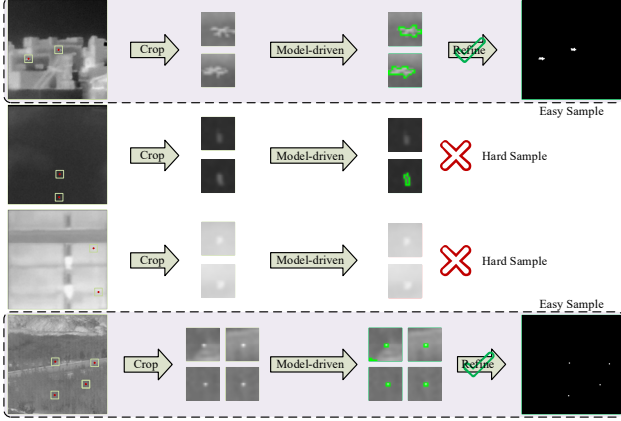


Figure 4. The EPG strategy. The green boxes denote correct detections. The red boxes denote error detections.

First, we need to determine hard samples in the preparation pool that the current model can recognize:

$$S = \begin{cases} I \in \text{Easy Sample} & \text{if } R_{\text{miss}} \leq T_{\text{miss}} \text{ and } R_{\text{false}} \leq T_{\text{false}} \\ I \in \text{Hard Sample} & \text{otherwise} \end{cases} \quad (1)$$

where R_{miss} and R_{false} denote the target-level missed detection rate and false detection rate. T_{miss} and T_{false} denote the corresponding thresholds. When there is an intersection between the true point label and the predicted target area, the target is detected correctly.

Second, the selected easy samples enter the false target elimination step. Specifically, the target area in the predicted image that does not have any intersection with the true point label is directly eliminated:

$$\hat{P}_b = P_b \setminus \{A_f \in P_b \mid \text{Intersection}(A_f, L_{\text{true}}) = \emptyset\} \quad (2)$$

where P_b and \hat{P}_b denote the detection results before and after eliminating the false detection area. A_f denotes the predicted target area. \setminus denotes the difference of sets. Intersection denotes the intersection area determination.

Finally, considering that there may be target omissions in the prediction results, we supplement the information with true point labels and output the final prediction map to ensure that no target learning is missed.

Considering that the model will have stronger cognitive and learning abilities after learning hard samples, we periodically perform COU during the training. This drives the model to progressively and actively recognize and learn more hard samples.

1) Fine inner updates (FIU): The pseudo-labels in the training pool are not fully refined. To solve this problem, we construct a FIU. It is inspired by [1] and effectively solves the potential problem of excessive label evolution as shown in the Supplementary Materials. The FIU is divided into three steps: candidate area extraction, false area elimination and pseudo-label update.

For candidate area extraction, we first obtain the binary

label for the n_{th} pseudo-label iteration. Second, the centroid of each target connected area in the pseudo-label is extracted and the corresponding $d \times d$ local area in the pseudo-label and prediction result is cropped. Finally, to highlight the target area and eliminate the accumulated error, we use adaptive thresholding to extract the local candidate areas in the prediction results:

$$C_n^i = (P_n^i > T_{\text{adapt}}) \quad (3)$$

$$T_{\text{adapt}} = \max(P_n^i)(T_b + k(1 - T_b)L_n^i / (\text{hwr})) \quad (4)$$

where C_n^i denotes candidate areas. P_n^i and L_n^i denote the prediction result and pseudo-label of the image patch. T_b and k are both set to 0.5 [1]. r is set to 0.15% [3, 32].

For false area elimination, similar to Eq.(2), we use the centroid of the target area in the pseudo-label to perform intersection judgments with the candidate areas. Candidate areas that do not have any intersections will be eliminated.

For pseudo-label update, we first restore the positions of all refined candidate areas and use the maximum method to combine them into complete candidate areas. Then, the pseudo-label is updated:

$$N_n = \max(\{N_n, \hat{C}_n^i\}) \quad (5)$$

$$L_{n+1} = \lambda L_n \odot (1 - N_n) + \frac{L_n + P_n}{2} \odot N_n \quad (6)$$

where λ is the decay factor. N_n is initialized to a zero matrix with the same size as the label. \hat{C}_n^i denotes the refined candidate areas of the image patch. P_n and L_n denote the prediction result and pseudo-label.

With the improvement of model capabilities and various constraints, the evolution of the target annotation area achieves a dynamic balance between expansion and contraction and generates more refined pseudo-labels.

3.5. Loss Function

For the SIRST detection task, the lack of intrinsic features makes it difficult to accurately locate the target area [9, 30, 31]. Therefore, we introduce an edge-enhanced difficulty-mining (EEDM) loss [52] to constrain the network optimization. This helps alleviate the imbalance problem of positive and negative pixels, and guides the network to pay more attention to difficult pixels and edge features during training. EEDM loss consists of two parts: edge pixel enhancement and difficult pixel mining. More results can be found in the Supplementary Materials.

4. Experiments

4.1. Datasets

Four public SIRST detection datasets are used in the experiments, namely SIRST3 [1], NUAA-SIRST [32], NUDT-SIRST [3], and IRSTD-1K [2]. They contain 2755, 427, 1327 and 1001 samples, respectively. We follow the

Table 1. IoU (%), nIoU (%), P_d (%) and F_a ($\times 10^{-6}$) values of different methods achieved on the SIRST3 dataset. *NUAA-SIRST-Test*, *NUDT-SIRST-Test* and *IRSTD-1K-Test* denote the decompositions of *SIRST3-Test* to verify the robustness of the model.

Scheme	Description	SIRST3-Test				NUAA-SIRST-Test				NUDT-SIRST-Test				IRSTD-1K-Test			
		IoU	nIoU	P_d	F_a	IoU	nIoU	P_d	F_a	IoU	nIoU	P_d	F_a	IoU	nIoU	P_d	F_a
FKRW ^[14]	Filtering	14.46	23.67	60.66	22.50	22.84	29.61	77.19	51.28	14.70	24.11	58.10	106.90	9.25	15.89	54.21	22.32
MPCM ^[18]	Local Contrast	18.54	26.80	71.96	123.76	42.92	46.48	88.59	91.08	12.55	20.46	64.34	550.90	21.36	26.78	81.48	191.34
NIPPS ^[24]	Low Rank	18.82	28.59	70.56	15.17	26.82	37.58	80.23	39.42	18.66	26.16	68.89	42.10	14.93	27.07	67.34	38.85
ACM ^[32]	CNN Full	64.93	64.89	94.88	20.97	67.61	67.57	92.02	10.36	65.77	65.65	95.87	15.95	61.92	59.55	94.28	28.07
	CNN Coarse + LESPS	37.42	35.20	84.12	50.13	43.66	41.51	84.41	37.94	37.22	33.01	83.91	41.09	34.09	35.73	84.51	60.98
	CNN Coarse + PAL (Ours)	51.51	54.07	92.89	39.18	58.66	60.09	87.07	24.49	54.47	54.42	94.50	15.21	42.75	46.50	92.93	63.05
ALCNet ^[30]	CNN Full	65.69	66.68	95.02	34.60	70.33	69.49	94.68	13.72	66.64	68.32	95.56	25.65	61.60	58.28	93.60	47.77
	CNN Coarse + LESPS	45.30	41.81	91.96	48.23	50.15	47.72	90.87	30.80	42.00	39.02	92.38	41.25	50.26	44.71	91.58	58.81
	CNN Coarse + PAL (Ours)	57.11	60.22	93.95	37.20	65.54	65.79	93.16	22.09	58.60	60.68	94.50	34.88	49.74	52.77	92.93	43.33
MLCL-Net ^[8]	CNN Full	78.44	82.01	95.22	17.99	71.28	74.38	91.25	34.57	89.36	90.11	97.14	13.44	63.25	63.38	92.59	17.16
	CNN Coarse + LESPS	40.83	38.34	87.64	45.21	47.73	44.91	91.25	34.44	38.81	35.14	86.46	37.71	41.27	41.90	88.21	54.37
	CNN Coarse + PAL (Ours)	64.87	69.40	94.95	24.43	66.63	70.04	93.54	24.08	71.20	72.65	97.14	21.28	51.11	57.96	89.23	25.03
ALCL-Net ^[9]	CNN Full	79.38	81.09	96.08	18.64	72.79	75.36	93.54	20.92	87.68	88.21	97.57	13.03	68.36	63.66	93.60	22.64
	CNN Coarse + LESPS	53.62	52.15	92.09	48.61	62.70	60.92	91.63	20.44	51.95	49.52	92.38	60.58	52.28	51.49	91.58	46.52
	CNN Coarse + PAL (Ours)	66.29	68.18	94.75	18.79	66.56	69.09	91.63	28.88	68.95	70.58	96.83	16.20	60.75	59.29	90.91	18.14
DNANet ^[3]	CNN Full	81.96	85.90	97.54	9.11	78.06	80.50	97.72	15.71	92.70	93.37	99.05	5.77	64.80	66.94	92.59	10.04
	CNN Coarse + LESPS	57.52	55.09	91.30	19.04	61.80	61.32	92.40	13.03	57.65	53.41	93.44	18.66	54.56	54.02	83.50	21.01
	CNN Coarse + PAL (Ours)	67.20	70.20	96.15	10.86	70.35	71.99	95.82	24.28	70.72	72.61	98.62	7.47	57.33	60.33	88.55	9.94
GGL-Net ^[10]	CNN Full	82.06	85.34	97.74	12.76	78.40	79.99	96.96	20.72	92.07	92.34	99.26	4.87	66.68	67.88	93.60	17.08
	CNN Coarse + LESPS	58.98	57.16	94.75	20.47	66.26	64.80	95.06	20.72	57.81	54.69	95.45	13.56	57.32	57.18	92.26	26.11
	CNN Coarse + PAL (Ours)	68.52	71.69	97.14	16.69	71.21	74.02	95.44	17.42	72.02	73.92	98.52	6.50	59.90	61.86	94.61	24.90
UIUNet ^[33]	CNN Full	83.14	85.29	97.34	15.44	76.64	78.43	95.82	12.69	92.94	93.29	98.41	4.11	70.04	66.19	95.29	25.55
	CNN Coarse + LESPS	52.43	52.86	93.09	16.92	58.55	60.66	90.11	20.37	52.03	50.20	94.50	12.18	49.71	53.35	91.25	19.87
	CNN Coarse + PAL (Ours)	69.05	71.53	96.81	15.45	66.05	69.21	93.54	10.98	74.21	75.61	98.52	9.15	60.63	60.50	94.28	21.90
MSDA-Net ^[31]	CNN Full	83.46	85.97	97.41	17.15	74.81	78.61	95.06	30.94	93.62	94.03	99.26	9.67	70.98	67.16	93.60	19.51
	CNN Coarse + LESPS	46.26	45.73	85.38	36.16	54.91	54.69	92.02	30.25	45.18	42.48	83.92	35.32	43.16	46.92	84.18	38.49
	CNN Coarse + PAL (Ours)	69.38	71.55	97.41	16.34	71.67	73.38	96.96	11.59	72.62	73.86	98.41	6.18	61.62	61.94	94.61	26.04

partitioning in [1, 3] for NUAA-SIRST and NUDT-SIRST and follow the partitioning in [1, 2] for IRSTD-1K. The stability of the proposed framework under few samples can be explored on these three datasets. SIRST3 is a multi-sample, multi-scene, and multi-target dataset that combines NUAA-SIRST, NUDT-SIRST, and IRSTD-1K. It can more effectively explore the model's comprehensive detection capabilities. Consistent with [1], we process the training set labels into two types: *Coarse* point labels and *Centroid* point labels.

4.2. Implementation Details

Experimental Settings: We use the AdamW [53] optimizer with initial learning rate as 1.0×10^{-3} to train the model. The batch size is set to 16. The total training epochs is 400, which is divided into 3 parts: 0-0.2, 0-0.8 and 0.8-1. To ensure that all samples can be learned, the initial missed detection rate threshold is set to 0.2 and increases linearly to 1 during the model enhancement phase. During training, all images are normalized and randomly cropped into 256×256 pixel patches as network inputs.

Evaluation Metrics: We used two pixel-level evaluation metrics of intersection over union (IoU) and normalized IoU (nIoU) [32] and two target-level evaluation metrics of detection probability (P_d) and false alarm rate F_a [3]. In addition, since the magnitude of F_a is 10^{-6} , its value is small and prone to fluctuations. Therefore, another reasonable comparison method is to convert it into a threshold evaluation metric. The model is valid when F_a is greater than $1e^{-4}$ [50, 54]. Red denotes the model is invalid.

4.3. Comparison with SOTA Methods

We embed several excellent SIRST detection networks [3, 8-10, 30-33] into our framework. For fair comparison, we retrain all models with the same settings. Meanwhile, we also conduct detailed comparative experiments with various traditional methods [14, 18, 24] and the latest LESPS framework [1]. More results can be found in the Supplementary Materials.

Evaluation on the SIRST3 dataset. From Table 1, when the networks (UIU-Net, MSDA-Net) are embedded into the LESPS framework for single point supervision tasks, they fail to exert their performance advantages on full supervision. The reason is that the LESPS framework directly trains all point labels and starts label evolution when the loss drops to a fixed value or reaches a fixed epoch. However, none of these conditions can accurately control the timing of good initial evolution. Our PAL framework can effectively solve this problem. The performance trend of CNNs equipped with the PAL framework on single point supervision is basically consistent with that of full supervision. The PAL framework can build an efficient and stable bridge between full supervision and single-point supervision tasks. At the same time, compared with the LESPS framework, using our PAL framework improves the IoU by 9.68%-24.04%, the nIoU by 14.53%-31.06%, and the P_d by 1.99%-12.03% on the comprehensive SIRST3-Test. The improvement is very obvious. Compared with the fully supervised task on the SIRST3-Test, our PAL framework can reach 79.33%-86.94% on IoU, 81.72%-90.30% on nIoU, and has

Table 2. IoU (%), nIoU (%), P_d (%) and F_a ($\times 10^{-6}$) values of different methods achieved on the separate NUAAs-SIRST, NUDTs-SIRST, and IRSTD-1k datasets. (213:214), (663:664) and (800:201) denote the division of training samples and test samples.

Scheme	Description	NUAA-SIRST (213:214)				NUDT-SIRST (663:664)				IRSTD-1K (800:201)			
		IoU	nIoU	P_d	F_a	IoU	nIoU	P_d	F_a	IoU	nIoU	P_d	F_a
ACM [32]	CNN Full	65.67	63.74	90.11	24.01	65.33	65.12	95.87	12.92	60.45	53.70	92.26	46.06
ALCNet [30]	CNN Full	66.41	65.18	91.63	35.26	69.74	70.67	97.46	11.15	62.47	55.25	88.89	36.79
MLCL-Net [8]	CNN Full	74.68	76.50	95.82	28.74	94.03	93.97	98.73	7.721	64.86	63.35	91.25	23.23
	CNN Coarse + LESPS	41.31	41.13	90.87	43.22	53.55	48.70	90.05	21.92	44.64	42.04	88.22	36.42
	CNN Coarse + PAL (Ours)	68.76	70.75	93.92	39.10	74.00	73.71	95.45	9.40	58.90	58.79	90.91	24.63
ALCL-Net [9]	CNN Full	72.84	72.59	95.06	17.01	92.80	93.01	99.05	2.21	65.56	65.03	91.58	9.68
	CNN Coarse + LESPS	37.99	41.91	90.87	35.54	45.89	43.66	90.48	34.45	49.46	45.00	82.49	26.72
	CNN Coarse + PAL (Ours)	67.49	67.67	93.54	24.01	70.62	72.56	98.31	7.93	57.98	53.36	88.22	20.61
DNANet [3]	CNN Full	76.40	78.32	96.20	20.72	95.17	95.19	98.94	2.00	69.06	65.22	91.58	11.56
	CNN Coarse + LESPS	9.29	7.36	19.77	415.72	48.10	48.84	81.80	85.19	50.99	47.61	85.52	25.49
	CNN Coarse + PAL (Ours)	66.57	69.73	90.49	27.44	73.29	74.70	98.10	22.08	58.40	60.29	91.25	24.52
GGL-Net [10]	CNN Full	75.47	75.93	97.34	20.65	94.86	94.93	99.47	1.03	69.09	65.52	92.59	13.68
	CNN Coarse + LESPS	55.17	54.51	89.35	26.27	57.39	56.67	91.75	23.92	50.90	48.12	86.20	27.73
	CNN Coarse + PAL (Ours)	63.46	64.31	90.11	25.73	73.10	74.83	98.20	13.12	60.72	57.05	90.24	40.20
UIUNet [33]	CNN Full	78.02	76.85	96.58	14.68	95.07	95.10	98.73	0.21	70.94	64.32	91.25	10.57
	CNN Coarse + LESPS	7.11	8.02	72.62	550.80	35.89	33.12	78.41	89.05	21.49	18.29	73.74	227.06
	CNN Coarse + PAL (Ours)	62.25	61.68	91.25	34.99	74.89	76.11	98.62	7.10	61.70	59.99	92.57	21.60
MSDA-Net [31]	CNN Full	76.73	77.78	96.20	21.75	95.27	95.18	99.15	1.72	70.98	65.70	93.94	33.95
	CNN Coarse + LESPS	43.39	49.33	88.59	27.37	41.60	38.25	79.79	34.42	43.29	38.16	83.16	54.98
	CNN Coarse + PAL (Ours)	66.78	65.92	92.78	22.77	74.48	75.37	97.46	16.80	62.72	56.71	89.23	28.64

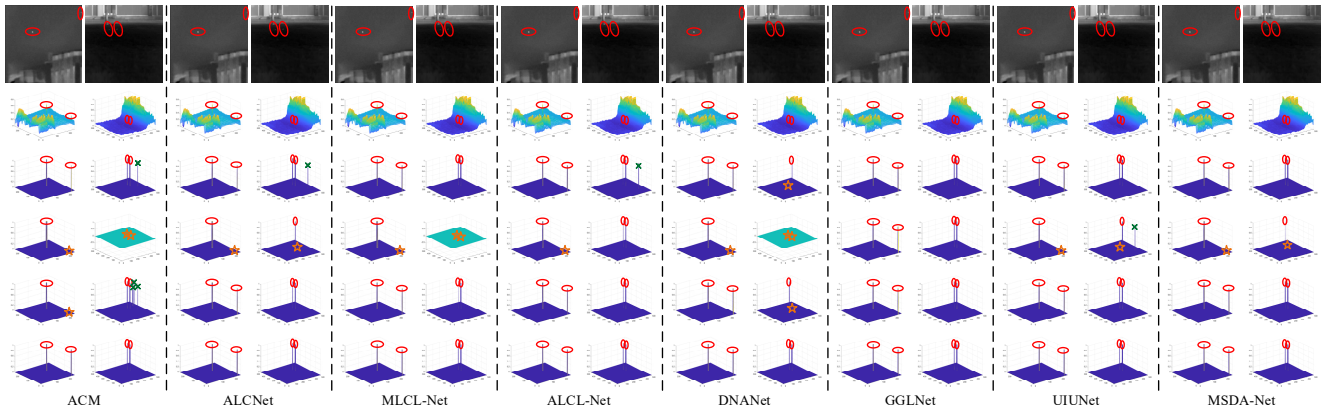


Figure 5. 3D visualization on the SIRST3 dataset. The circles denote correct detections, the crosses denote false detections, and the stars denote missed detections. From top to bottom: 2D image, 3D image, CNN Full, CNN Coarse + LESPS, CNN Coarse + PAL, True label.

comparable performance on P_d . In addition, by observing the results on the three decomposed test subsets, our PAL framework has stable performance. Furthermore, from Fig. 5, CNNs equipped with the PAL framework have target-level detection effects similar to those of full supervision, and they are significantly better than the LESPS framework.

Evaluation on three individual datasets. To further explore the stability of our PAL framework when there are few training samples, we perform separate training and testing on the three individual datasets. From Table 2, the PAL framework is significantly better than the LESPS framework. Meanwhile, the performance of our PAL framework is stable. These results show that the PAL framework can solve the single point supervised SIRST detection task with few training samples, whereas the LESPS framework has a significant risk of failure. Specifically, compared with the LESPS framework, using the PAL framework improves the IoU by 7.41%-57.28%, the nIoU by 8.36%-62.37%, and the P_d by 0.76%-70.72%.

4.4. Ablation Experiment

1) Break-Down Ablation. To verify the effectiveness of model pre-start and fine dual-update strategy, Table 3 presents detailed ablation experiments. From Scheme 1 and Scheme 2, training directly with point labels will fail, but the network after applying the model pre-start will show significant performance improvement. This verifies the effectiveness of our model pre-start concept and EPG strategy. From Schemes 2-4, whether using COU or FIU alone can significantly improve the performance. In addition, from Schemes 2-5, when the COU and the FIU are used in combination, a significant performance improvement of "1+1>2" is achieved. This fully verifies the effectiveness of the proposed fine dual-update strategy.

2) Decay Factor. As presented in Table 4, compared with not using the decay factor ($\alpha=1$), using decay factors can improve the segmentation accuracy. The IoU will increase by 0.04%-1.48% and the nIoU will increase by 1.10%-2.92%. At the same time, using a decay factor

Table 3. Break-down ablation experiments on the SIRST3 dataset. *MP* is the model pre-start. *Coarse* denotes coarse point supervision. *Centroid* denotes centroid point supervision.

Scheme	Variants			MSDA-Net Coarse + PAL				MSDA-Net Centroid + PAL			
	MP	COU	FIU	IoU	nIoU	P _d	F _a	IoU	nIoU	P _d	F _a
Scheme1	-	-	-	1.23	2.60	40.47	0.26	2.56	4.94	83.52	0.61
Scheme2	✓	✗	✗	56.24	64.20	89.63	31.48	57.25	64.44	91.83	23.83
Scheme3	✓	✓	✗	61.64	67.14	94.02	31.15	60.19	67.17	95.75	18.74
Scheme4	✓	✗	✓	61.66	66.78	93.42	39.47	59.81	65.38	92.89	25.06
Scheme5	✓	✓	✓	69.38	71.55	97.41	16.34	69.21	72.40	97.01	15.70

Table 4. Decay factor investigation on the SIRST3 dataset.

α	MSDA-Net Coarse + PAL					α	MSDA-Net Coarse + PAL				
	IoU	nIoU	P _d	F _a	IoU		nIoU	P _d	F _a		
1.00	67.90	69.67	96.68	18.96	0.95	68.96	71.40	97.41	15.76		
0.99	68.02	70.94	96.74	19.13	0.90	68.92	72.00	96.48	16.35		
0.98	68.92	71.20	96.88	19.02	0.85	68.73	72.59	96.41	18.66		
0.97	69.38	71.55	97.41	16.34	0.80	67.94	71.30	96.15	20.36		
0.96	69.13	70.77	97.28	16.52	0.75	68.11	71.60	95.55	29.45		

Table 5. Comparison of different losses on the SIRST3 dataset.

Loss Function	MSDA-Net Coarse + PAL				MSDA-Net Centroid + PAL			
	IoU	nIoU	P _d	F _a	IoU	nIoU	P _d	F _a
BCE loss	69.26	71.48	97.08	15.98	69.19	71.67	96.74	14.25
Dice loss	64.38	66.64	94.68	39.83	65.18	67.71	95.61	35.61
Focal loss	68.89	72.21	97.01	17.02	69.14	71.85	96.28	16.18
EEDM loss	69.38	71.55	97.41	16.34	69.21	72.40	97.01	15.70

Table 6. Comparison of the PAL framework with different settings on the SIRST3 dataset. *MP* denotes the proposed model pre-start. *MP-1* and *MP-2* denote the model pre-start with all samples initially enter the training pool by setting the target recall threshold to 0 and directly carry the true point labels for remaining hard samples into the training pool. *S* denotes scheme.

S	Variants			MSDA-Net Coarse + PAL				MSDA-Net Centroid + PAL					
	MP	MP-1	MP-2	COU	FIU	IoU	nIoU	P _d	F _a	IoU	nIoU	P _d	F _a
S1	✓	✗	✗	✗	✗	56.24	64.20	89.63	31.48	57.25	64.44	91.83	23.83
S2	✗	✓	✗	✗	✗	32.86	45.42	73.62	13.62	32.45	44.18	73.49	13.19
S3	✗	✗	✓	✗	✗	25.72	38.26	61.53	14.14	28.77	41.86	71.56	11.67
S4	✓	✗	✗	✗	✓	61.66	66.78	93.42	39.47	59.81	65.38	92.89	25.06
S5	✗	✓	✗	✗	✓	40.84	51.23	74.82	18.88	41.87	52.96	78.80	14.15
S6	✗	✗	✓	✗	✓	36.67	48.88	71.10	12.10	37.13	48.75	75.08	11.37
S7	✓	✗	✗	✓	✓	69.38	71.55	97.41	16.34	69.21	72.40	97.01	15.70

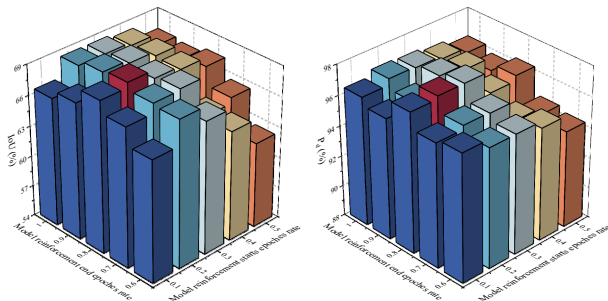


Figure 6. Epoch division investigation on the SIRST3 dataset. Red denotes the optimal value.

within a reasonable range will also lead to an increase in P_d. We finally set α to 0.97.

3) Epochs Division. As presented in Fig. 6, when the model pre-start interval is greater than 0.1 and the model enhancement interval is from 0.1 to 0.4, the performance

shows an upward trend. This shows that subdividing all the hard samples multiple times will have a more positive performance improvement. It is like a student model with basic abilities breaking down the final learning goal into multiple steps, and then learning from easy to hard. This is effective both intuitively and from experimental results. At the same time, when the model refinement phase is eliminated or the model pre-start interval is only 0.1, the performance of the network will degrade. This proves the superiority of the 3-phase design in our PAL framework. In addition, when the model pre-start interval is greater than 0.1 and the model enhancement interval is greater than 0.3, the performance is stable. It demonstrates the robustness of our PAL framework.

4) Loss Function. We compare EEDM loss with the binary cross-entropy loss, Dice loss [55] and focal loss [56]. From Table 5, compared with other losses, EEDM loss has the best results. Using EEDM loss can improve the IoU by 0.02%-5.00% and improve the P_d by 0.33%-2.73%.

4.5. Discussion of “From easy to hard”

To further discuss the proposed progressive active learning idea that focuses on learning from easy samples to hard samples, we conduct detailed experiments. From S1-S6 in Table 6, regardless of whether FIU are added or not, the final model generated by all samples entering the training pool in the initial stage is far worse than that of using only easy samples. This further verifies the effectiveness of our model pre-start concept of learning only easy samples in the initial phase. It's like babies should be given pronunciation exercises rather than forced to learn calculus. In addition, from S4 and S6 in Table 6, compared to using only easy samples, gradually selecting hard samples into the training pool based on the current capabilities will again achieve significant performance improvements. This further verifies the effectiveness of the idea of learning from easy samples to hard samples.

5. Conclusion

This paper proposes an innovative PAL framework for the SIRST detection with single point supervision, which focuses on learning from easy samples to hard samples. First, we propose a model pre-start concept, which can help models have basic task-specific learning capabilities in the initial training phase. Second, a refined dual-update strategy is proposed, which can promote reasonable learning of harder samples and continuous refinement of pseudo-labels. Finally, to alleviate the risk of region expansion without shrinkage, a decay factor is reasonably introduced to achieve a dynamic balance between the expansion and shrinkage of target annotations. Extensive comparison results demonstrate the superiority of our PAL framework. We hope that our study can draw attention to the research on weakly supervised SIRST detection.

References:

- [1] Xinyi Ying, Li Liu, Yingqian Wang, Ruoqing Li, Nuo Chen, Zaiping Lin, Weidong Sheng, and Shilin Zhou. Mapping Degeneration meets label evolution: Learning infrared small target detection with single point supervision. In *Proceedings of the IEEE Conference on Computer Vision and Pattern Recognition (CVPR)*, pages 15528-15538, 2023. 1, 3, 4, 5, 6.
- [2] Mingjin Zhang, Rui Zhang, Yuxiang Yang, Haichen Bai, Jing Zhang, and Jie Guo. ISNet: Shape matters for infrared small target detection. In *Proceedings of the IEEE Conference on Computer Vision and Pattern Recognition (CVPR)*, pages 867-876, 2022. 1, 2, 5.
- [3] Boyang Li, Chao Xiao, Longguang Wang, Yingqian Wang, Zaiping Lin, Miao Li, Wei An, and Yulan Guo. Dense nested attention network for infrared small target detection. *IEEE Transactions on Image Processing*, 32: 1745-1758, 2023. 1, 2, 4, 5, 6.
- [4] Yangsheng Li and Yongjun Zhang. Robust infrared small target detection using local steering kernel reconstruction. *Pattern Recognition*, 77: 113-125, 2018. 1.
- [5] Hai Xu, Sheng Zhong, Tianxu Zhang, and Xu Zou. Multiscale multilevel residual feature fusion for real-time infrared small target detection. *IEEE Transactions on Geoscience and Remote Sensing*, 61: 1-16, 2023. 1.
- [6] Mingjin Zhang, Ke Yue, Jing Zhang, Yunsong Li, and Xinbo Gao. Exploring feature compensation and cross-level correlation for infrared small target detection. In *Proceedings of the 30th ACM International Conference on Multimedia (ACM MM)*, pages 1857-1865, 2022. 1.
- [7] Enzhong Zhao, Lili Dong, Chenxi Li, and Yingjie Ji. Infrared maritime target detection based on temporal weight and total variation regularization under strong wave interferences. *IEEE Transactions on Geoscience and Remote Sensing*, 62: 1-19, 2024. 1.
- [8] Chuang Yu, Yunpeng Liu, Shuhang Wu, Zhuhua Hu, Xin Xia, Deyan Lan, and Xin Liu. Infrared small target detection based on multiscale local contrast learning networks. *Infrared Physics & Technology*, 123, 2022. 1, 6, 7.
- [9] Chuang Yu, Yunpeng Liu, Shuhang Wu, Xin Xia, Zhuhua Hu, Deyan Lan, and Xin Liu. Pay attention to local contrast learning networks for infrared small target detection. *IEEE Geoscience and Remote Sensing Letters*, 19: 1-5, 2022. 1, 2, 5, 6, 7.
- [10] Jinmiao Zhao, Chuang Yu, Zelin Shi, Yunpeng Liu, and Yingdi Zhang. Gradient-guided learning network for infrared small target detection. *IEEE Geoscience and Remote Sensing Letters*, 20: 1-5, 2023. 1, 2, 6, 7.
- [11] Gonzalo R. Arce and Michael McLoughlin. Theoretical analysis of the max/median filter. *IEEE Transactions on Acoustics, Speech, and Signal Processing*, 35(1): 60-69, 1987. 1, 2.
- [12] Xiangzhi Bai and Fugen Zhou. Analysis of new top-hat transformation and the application for infrared dim small target detection. *Pattern Recognition*, 43(6): 2145-2156, 2010. 1, 2.
- [13] Carlo Tomasi and Roberto Manduchi. Bilateral filtering for gray and color images. In *Proceedings of the IEEE International Conference on Computer Vision (ICCV)*, pages 839-846, 1998. 1, 2.
- [14] Yao Qin, Lorenzo Bruzzone, Chengqiang Gao, and Biao Li. Infrared small target detection based on facet kernel and random walker. *IEEE Transactions on Geoscience and Remote Sensing*, 57(9): 7104-7118, 2019. 1, 2, 6.
- [15] Zhong Chen, Song Luo, Ting Xie, Jianguo Liu, Guoyou Wang, and Gao Lei. A novel infrared small target detection method based on BEMD and local inverse entropy. *Infrared Physics & Technology*, 66: 114-124, 2014. 1, 2.
- [16] Baojun Qi, Tao Wu, and Hangen He. Robust detection of small infrared objects in maritime scenarios using local minimum patterns and spatio-temporal context. *Optical Engineering*, 51(2), 2012. 1, 2.
- [17] C. L. Philip Chen, Hong Li, Yantao Wei, Tian Xia, and Yuan Yan Tang. A local contrast method for small infrared target detection. *IEEE Transactions on Geoscience and Remote Sensing*, 52(1): 574-581, 2014. 1, 2.
- [18] Yantao Wei, Xinge You, and Hong Li. Multiscale patch-based contrast measure for small infrared target detection. *Pattern Recognition*, 58: 216-226, 2016. 1, 2, 6.
- [19] He Deng, Xianping Sun, Maili Liu, Chaohui Ye, and Xin Zhou. Small infrared target detection based on weighted local difference measure. *IEEE Transactions on Geoscience and Remote Sensing*, 54(7): 4204-4214, 2016. 1, 2.
- [20] Xiangzhi Bai and Yanguang Bi. Derivative entropy-based contrast measure for infrared small-target detection. *IEEE Transactions on Geoscience and Remote Sensing*, 56(4): 2452-2466, 2018. 1, 2.
- [21] Chenqiang Gao, Deyu Meng, Yi Yang, Yongtao Wang, Xiaofang Zhou, and Alexander G. Hauptmann. Infrared patch-image model for small target detection in a single image. *IEEE Transactions on Image Processing*, 22(12): 4996-5009, 2013. 1, 2.
- [22] Yujie He, Min Li, Jinli Zhang, and Qi An. Small infrared target detection based on low-rank and sparse representation. *Infrared Physics & Technology*, 68: 98-109, 2015. 1, 2.
- [23] Landan Zhang, Lingbing Peng, Tianfang Zhang, Siying Cao, and Zhenming peng. Infrared small target detection via non-convex rank approximation minimization joint l_2, l_1 norm. *Remote Sensing*, 10(11), 2018. 1, 2.
- [24] Yimian Dai, Yiquan Wu, and Yu Song. Non-negative infrared patch-image model: Robust target-background separation via partial sum minimization of singular values. *Infrared Physics & Technology*, 81: 182-194, 2017. 1, 2, 6.
- [25] Yann LeCun, Yoshua Bengio, and Geoffrey Hinton. Deep learning. *Nature*, 521: 436-444, 2015. 1.
- [26] Joseph Redmon, Santosh Divvala, Ross Girshick, and Ali Farhadi. You only look once: Unified, real-time object detection. In *Proceedings of the IEEE Conference on Computer Vision and Pattern Recognition (CVPR)*, pages 779-788, 2016. 1.
- [27] Joseph Redmon, and Ali Farhadi. YOLO9000: Better, faster, stronger. In *Proceedings of the IEEE Conference on Computer Vision and Pattern Recognition (CVPR)*, pages 6517-6525, 2017. 1.
- [28] Ao Wang, Hui Chen, Lihao Liu, Kai Chen, Zijia Lin, Jungong Han, and Guiguang Ding. YOLOv10: Real-time end-to-end object detection. *arXiv preprint arXiv:2405.14458*, 2024. 1.
- [29] Wei Liu, Dragomir Anguelov, Dumitru Erhan, Christian Szegedy, Scott Reed, Cheng-Yang Fu, and Alexander C. Berg. SSD: Single shot multibox detector. In *Proceedings of*

- the *European Conference on Computer Vision (ECCV)*, pages 21-37, 2016. 1
- [30] Yimian Dai, Yiquan Wu, Fei Zhou, and Kobus Barnard. Attentional local contrast networks for infrared small target detection. *IEEE Transactions on Geoscience and Remote Sensing*, 59(11): 9813-9824, 2021. 1, 2, 4, 5, 6, 7
- [31] Jinmiao Zhao, Zelin Shi, Chuang Yu, and Yunpeng Liu. Multi-scale direction-aware network for infrared small target detection. *arXiv preprint arXiv:2406.02037*, 2024. 1, 2, 4, 5, 6, 7
- [32] Yimian Dai, Yiquan Wu, Fei Zhou, and Kobus Barnard. Asymmetric contextual modulation for infrared small target detection. In *Proceedings of the Winter Conference on Applications of Computer Vision (WACV)*, pages 950-959, 2021. 2, 5, 6, 7
- [33] Xin Wu, Danfeng Hong, and Jocelyn Chanussot. UIU-Net: U-Net in U-Net for infrared small object detection. *IEEE Transactions on Image Processing*, 32: 364-376, 2023. 2, 6, 7
- [34] Amy Bearman, Olga Russakovsky, Vittorio Ferrari, and Fei-Fei Li. What's the point: Semantic segmentation with point supervision. In *Proceedings of the European Conference on Computer Vision (ECCV)*, pages 549-565, 2016. 2
- [35] Dim P. Papadopoulos, Jasper R. R. Uijlings, Frank Keller, and Vittorio Ferrari. Training object class detectors with click supervision. In *Proceedings of the IEEE Conference on Computer Vision and Pattern Recognition (CVPR)*, pages 180-189, 2017. 2
- [36] Shilong Zhang, Zhuoran Yu, Liyang Liu, Xinjiang Wang, Aojun Zhou, and Kai Chen. Group R-CNN for weakly semi-supervised object detection with points. In *Proceedings of the IEEE Conference on Computer Vision and Pattern Recognition (CVPR)*, pages 9407-9416, 2022. 2
- [37] Liangyu Chen, Tong Yang, Xiangyu Zhang, Wei Zhang, and Jian Sun. Points as queries: Weakly semi-supervised object detection by points. In *Proceedings of the IEEE Conference on Computer Vision and Pattern Recognition (CVPR)*, pages 8819-8828, 2021. 2
- [38] Issam H Laradji, Negar Rostamzadeh, and Pedro O Pinheiro, David Vazquez, and Mark Schmidt. Where are the blobs: Counting by localization with point supervision. In *Proceedings of the European Conference on Computer Vision (ECCV)*, pages 560-576, 2018. 2
- [39] Peri Akiva, Kristin Dana, Peter Oudemans, and Michael Mars. Finding berries: Segmentation and counting of cranberries using point supervision and shape priors. In *Proceedings of the IEEE/CVF Conference on Computer Vision and Pattern Recognition Workshops (CVPRW)*, pages 50-51, 2020. 2
- [40] Mohsen Zand, Haleh Damirchi, Andrew Farley, Mahdiyar Molahasani, Michael Greenspan, and Ali Etemad. Multiscale crowd counting and localization by multitask point supervision. In *Proceedings of the IEEE International Conference on Acoustics, Speech and Signal Processing (ICASSP)*, pages 1820-1824, 2022. 2
- [41] Shiyin Zhang, Jun Hao Liew, Yunchao Wei, Shikui Wei, and Yao Zhao. Interactive object segmentation with insideoutside guidance. In *Proceedings of the IEEE Conference on Computer Vision and Pattern Recognition (CVPR)*, pages 12234-12244, 2020. 2
- [42] Bowen Cheng, Omkar Parkhi, and Alexander Kirillov. Pointly-supervised instance segmentation. In *Proceedings of the IEEE Conference on Computer Vision and Pattern Recognition (CVPR)*, pages 2617-2626, 2022. 2
- [43] Junsong Fan, Zhaoxiang Zhang, and Tieniu Tan. Pointly supervised panoptic segmentation. *arXiv preprint arXiv:2210.13950*, 2022. 2
- [44] Kevis-Kokitsi Maninis, Sergi Caelles, Jordi Pont-Tuset, and Luc Van Gool. Deep extreme cut: From extreme points to object segmentation. In *Proceedings of the IEEE Conference on Computer Vision and Pattern Recognition (CVPR)*, pages 616-625, 2018. 2
- [45] Rui Qian, Yunchao Wei, Honghui Shi, Jiachen Li, Jiaying Liu, and Thomas Huang. Weakly supervised scene parsing with point-based distance metric learning. In *Proceedings of the AAAI Conference on Artificial Intelligence (AAAI)*, pages 8843-8850, 2019. 2
- [46] Anan Du, Tianfei Zhou, Shuchao Pang, Qiang Wu, and Jian Zhang. PCL: Point contrast and labeling for weakly supervised point cloud semantic segmentation. *IEEE Transactions on Multimedia*, 26: 8902-8914, 2024. 2
- [47] Yachao Zhang, Yanyun Qu, Yuan Xie, Zonghao Li, Shanshan Zheng, and Cuihua Li. Perturbed self-distillation: weakly supervised large-scale point cloud semantic segmentation. In *Proceedings of the IEEE International Conference on Computer Vision (ICCV)*, pages 15500-15508, 2021. 2
- [48] Jiacheng Wei, Guosheng Lin, Kim-Hui Yap, Tzu-Yi Hung, and Lihua Xie. Multi-path region mining for weakly supervised 3D semantic segmentation on point clouds. In *Proceedings of the IEEE Conference on Computer Vision and Pattern Recognition (CVPR)*, pages 4383-4392, 2020. 2
- [49] Yonghao Xu and Pedram Ghamisi. Consistency-regularized region-growing network for semantic segmentation of urban scenes with point-level annotations. *IEEE Transactions on Image Processing*, 31: 5038-5051, 2022. 2
- [50] Jinmiao Zhao, Zelin Shi, Chuang Yu, and Yunpeng Liu. Refined infrared small target detection scheme with single-point supervision. *arXiv preprint arXiv:2408.02773*, 2024. 4, 6
- [51] John Canny. A Computational Approach to Edge Detection. *IEEE Transactions on Pattern Analysis and Machine Intelligence*, PAMI-8(6): 679-698, 1986. 4
- [52] Jinmiao Zhao, Zelin Shi, Chuang Yu, and Yunpeng Liu. Infrared small target detection based on adjustable sensitivity strategy and multi-scale fusion. *arXiv preprint arXiv:2407.20090*, 2024. 5
- [53] Ilya Loshchilov and Frank Hutter. Decoupled weight decay regularization. *arXiv preprint arXiv:1711.05101*, 2017. 6
- [54] Chuang Yu, Yunpeng Liu, Jinmiao Zhao, and Zelin Shi. LR-Net: A lightweight and robust network for infrared small target detection. *arXiv preprint arXiv:2408.02780*, 2024. 6
- [55] Fausto Milletari, Nassir Navab, and Seyed-Ahmad Ahmadi. V-Net: Fully convolutional neural networks for volumetric medical image segmentation. In *Proceedings of the International Conference on 3D Vision (3DV)*, pages 565-571, 2016. 8
- [56] Tsung-Yi Lin, Priya Goyal, Ross Girshick, Kaiming He, and Piotr Dollár. Focal loss for dense object detection. *IEEE Transactions on Pattern Analysis and Machine Intelligence*, 42(2): 318-327, 2020. 8

From Easy to Hard: Progressive Active Learning Framework for Infrared Small Target Detection with Single Point Supervision

Supplementary Material

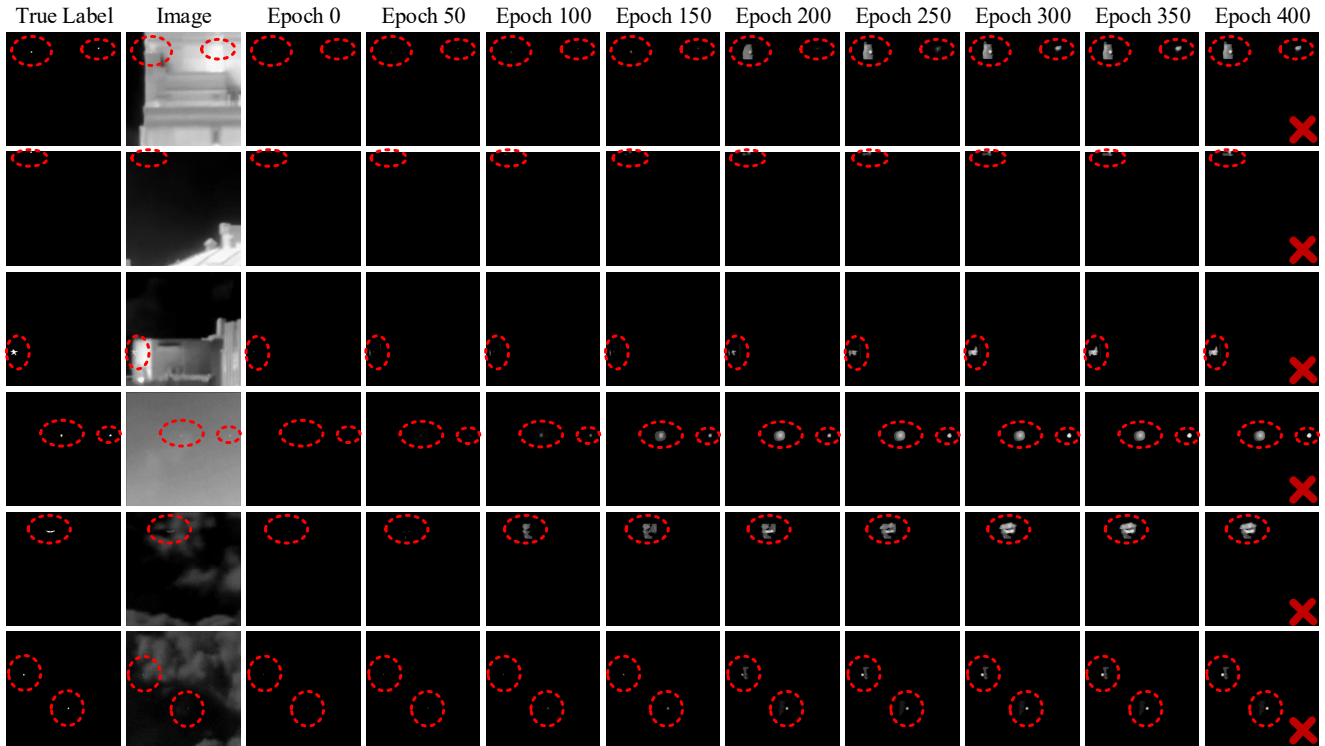


Figure 1. Label evolution results of MSDA-Net equipped with the LESPS framework on the NUDT-SIRST dataset. As the number of epochs increases, the labelled area expands excessively and does not shrink, which will affect the final detection performance.

In this supplementary material, we offer extra details and additional results to complement the main paper. In Section A, we provide a presentation and analysis of the risk of excessive label evolution in the LESPS framework. In Section B, we provide a detailed introduction to the used edge-enhanced difficulty-mining (EEDM) loss. In Section C, we provide more ablation experiments to fully explore the performance of our proposed Progressive Active Learning (PAL) framework. In Section D, we provide more quantitative comparative experiments on different datasets. In Section E, we provide more qualitative results to further verify the superiority of the proposed PAL framework.

A. Excessive Label Evolution in the LESPS

In exploring the LESPS framework [1], we find that it has the risk of excessive label evolution. From Fig. 1, when using the LESPS framework, if the pseudo-label has an overly large annotation of the target area during evolution,

the area will not shrink, but will either remain the same or expand further. The reason is that the label evolution rule does not consider the shrinkage problem of the target annotation in the pseudo-label after it is too large. The LESPS framework is designed to generate reasonable candidate regions using an adaptive threshold rule, which effectively avoids cumulative errors. However, it can only prevent the continued large-scale expansion and cannot prevent the initial occurrence of errors. At the same time, it ignores the fact that the calculation of the adaptive threshold is based on the target area in the pseudo-label rather than the prediction result of the current iteration. Therefore, when the target annotation of the pseudo-label is small and the annotation of the current prediction result is too large, there is a risk of over-expansion in the target annotation of the updated pseudo-label. Since there is no design for shrinking the annotation area in its pseudo-label update strategy, an overly expanded annotation area cannot be shrunk. Therefore, to reduce the risk of excessive label evolution mentioned above, we introduce a decay factor,

Table 1: Batch size investigation on the SIRST3 dataset. *Coarse* denotes coarse point supervision. *Centroid* denotes centroid point supervision.

Batch size	MSDA-Net Coarse + PAL				MSDA-Net Centroid + PAL			
	IoU	nIoU	P _d	F _a	IoU	nIoU	P _d	F _a
40	67.33	70.90	96.41	20.27	67.31	70.18	96.48	28.77
32	68.03	71.30	97.28	18.67	68.43	71.60	96.08	14.89
24	70.31	71.53	95.15	13.78	69.16	71.98	95.55	7.82
16	69.38	71.55	97.41	16.34	69.21	72.40	97.01	15.70
8	68.60	71.12	96.61	24.20	68.83	71.84	96.48	14.88

Table 2: Update period investigation on the SIRST3 dataset. *Coarse* denotes coarse point supervision. *Centroid* denotes centroid point supervision.

Update period	MSDA-Net Coarse + PAL				MSDA-Net Centroid + PAL			
	IoU	nIoU	P _d	F _a	IoU	nIoU	P _d	F _a
1	66.35	68.21	95.88	29.37	64.61	47.27	82.66	41.45
3	70.01	70.65	96.68	20.18	69.65	71.51	97.41	13.62
5	69.38	71.55	97.41	16.34	69.21	72.40	97.01	15.70
7	69.04	71.79	96.88	15.06	68.53	72.11	97.01	22.07
10	68.57	71.80	97.08	14.38	68.33	71.16	96.94	26.89

Table 3: Learning rate investigation on the SIRST3 dataset. *Coarse* denotes coarse point supervision. *Centroid* denotes centroid point supervision.

Learning rate	MSDA-Net Coarse + PAL				MSDA-Net Centroid + PAL			
	IoU	nIoU	P _d	F _a	IoU	nIoU	P _d	F _a
1e ⁻²	-	-	-	-	-	-	-	-
5e ⁻³	69.53	71.69	97.81	17.13	68.61	70.21	96.88	19.81
1e ⁻³	69.38	71.55	97.41	16.34	69.21	72.40	97.01	15.70
5e ⁻⁴	68.83	70.71	95.88	16.23	69.24	72.34	96.35	23.05
1e ⁻⁴	65.31	70.87	94.88	16.94	65.41	70.09	95.02	18.07
5e ⁻⁵	59.68	65.70	92.09	19.38	61.64	67.33	94.49	19.14

Table 4: Missed detection rate threshold investigation on the SIRST3 dataset. *Coarse* denotes coarse point supervision. *Centroid* denotes centroid point supervision.

T_{miss}	MSDA-Net Coarse + PAL				MSDA-Net Centroid + PAL			
	IoU	nIoU	P _d	F _a	IoU	nIoU	P _d	F _a
Change	69.38	71.55	97.41	16.34	69.21	72.40	97.01	15.70
0.2	69.30	71.69	96.88	19.05	69.07	70.89	97.54	16.32
0.4	69.14	71.14	96.21	14.00	69.06	71.38	96.94	16.52
0.6	68.73	71.61	96.61	15.82	68.91	71.41	96.41	17.69
0.8	67.41	71.06	96.08	15.61	68.42	71.14	96.08	15.64

which helps achieve a dynamic balance between the expansion and contraction of target annotations.

B. The EEDM Loss

For the SIRST detection task, the lack of intrinsic features makes it difficult to accurately locate the target area [2-4]. Therefore, we introduce an edge-enhanced difficulty-mining (EEDM) loss [5] to constrain the network optimization. The EEDM loss consists of two parts: edge pixel enhancement and difficult pixel mining. Taking a single image as an example, firstly, we obtain the target edge contour in the binary pseudo-label. Secondly,

the binary cross-entropy loss is used to obtain the loss value of each pixel and form a loss matrix. Finally, we weight the edge contours extracted from the labels and apply this weighting matrix to the calculated loss matrix to obtain the loss value of each point after edge weighting. The expressions are as follows:

$$L_{ij} = W_{ij} \cdot (-T_{ij} \log(P_{ij}) + (1 - T_{ij}) \log(1 - P_{ij})) \quad (1)$$

$$W_{ij} = \alpha \cdot E_{ij} + (1 - E_{ij}) \quad (2)$$

where E_{ij} denotes the edge extracted from the binary pseudo-label, edge pixels are marked as 1 and non-edge pixels are marked as 0. P_{ij} denotes the prediction result. T denotes the pseudo-label after binarization. α is the edge weighting coefficient, which is set to 4 [5].

Subsequently, difficult pixel mining is performed. Firstly, the loss values of each point are sorted. Secondly, the set of loss values that are greater than or equal to the median is obtained. Finally, the final loss is obtained by calculating the mean loss of difficult pixels. The expressions are as follows:

$$L_{EEDM} = \frac{1}{|S|} \sum_{(i,j) \in S} L_{ij} \quad (3)$$

$$S = \{(i, j) \mid L_{ij} \geq \text{median}(L_{ij})\} \quad (4)$$

where L_{EEDM} is the final output, S is the difficult pixel set.

On the one hand, EEDM loss promotes the network to increase its sensitivity to target edges by using edge information as an additional constraint. On the other hand, it uses difficult pixel mining to help the model better focus on difficult-to-detect target areas, thereby preventing small targets from being submerged by the background.

C. More Ablation Experiments

In this section, we study more influencing factors in detail, including the batch size, update period of the refined dual-update strategy, learning rate, and missed detection rate threshold.

1) Batch size. To explore the impact of batch size on the performance of the final generated model, we explore the PAL framework with different batch size settings. From Table 1, when the batch size is set too large or too small, the final generated model will experience a slight performance degradation. Specifically, when the batch size is set too large, the number of model updates will be reduced and each update will be based on a large number of samples, making the gradient update smoother and reducing the randomness of the model, which makes the model more likely to overfit on the training data. When the batch size is set too small, each gradient update is based only on a small number of data samples, resulting in a large variance in the gradient estimate and large fluctuations in the gradient direction, which makes it easy to fall into a local optimum. In addition, on the whole, the final model with different batch size settings has relatively stable

Table 5. IoU (%), nIoU (%), P_d (%) and F_a ($\times 10^{-6}$) values of different methods achieved on the SIRST3 dataset with centroid point labels. *NUAA-SIRST-Test*, *NUDT-SIRST-Test* and *IRSTD-1K-Test* denote the decompositions of *SIRST3-Test* to verify the robustness of the model. *CNN Centroid* denotes CNN-based methods under centroid point supervision.

Scheme	Description	SIRST3-Test				NUAA-SIRST-Test				NUDT-SIRST-Test				IRSTD-1K-Test			
		IoU	nIoU	P_d	F_a	IoU	nIoU	P_d	F_a	IoU	nIoU	P_d	F_a	IoU	nIoU	P_d	F_a
ACM ^[6]	CNN Full	64.93	64.89	94.88	20.97	67.61	67.57	92.02	10.36	65.77	65.65	95.87	15.95	61.92	59.55	94.28	28.07
	CNN Centroid + LESPS	38.38	36.39	91.16	60.84	42.25	40.72	88.97	46.79	36.50	34.12	92.06	53.77	40.49	39.27	90.24	70.56
	CNN Centroid + PAL (Ours)	51.51	53.73	92.82	35.98	57.87	58.00	88.59	28.40	54.73	54.76	94.50	21.79	42.51	45.79	91.25	49.80
ALCNet ^[3]	CNN Full	65.69	66.68	95.02	34.60	70.33	69.49	94.68	13.72	66.64	68.32	95.56	25.65	61.60	58.28	93.60	47.77
	CNN Centroid + LESPS	46.48	43.82	89.44	38.72	52.27	50.36	89.73	36.84	44.62	41.32	89.10	25.53	47.19	45.11	90.24	50.14
	CNN Centroid + PAL (Ours)	55.01	57.93	93.94	31.63	62.51	64.42	90.87	28.74	58.43	58.46	94.71	23.81	44.78	49.29	91.92	38.89
MLCL-Net ^[10]	CNN Full	78.44	82.01	95.22	17.99	71.28	74.38	91.25	34.57	89.36	90.11	97.14	13.44	63.25	63.38	92.59	17.16
	CNN Centroid+ LESPS	37.28	36.95	90.90	45.13	40.29	40.51	89.73	49.39	35.25	35.08	92.06	43.36	40.72	39.34	88.22	45.42
	CNN Centroid + PAL (Ours)	66.38	69.25	95.08	15.94	67.25	69.70	93.16	20.99	71.73	72.44	97.25	8.80	54.89	58.24	89.90	20.44
ALCL-Net ^[2]	CNN Full	79.38	81.09	96.08	18.64	72.79	75.36	93.54	20.92	87.68	88.21	97.57	13.03	68.36	63.66	93.60	22.64
	CNN Centroid + LESPS	55.63	54.13	94.15	26.29	59.99	60.30	93.92	20.79	56.03	52.49	94.92	13.67	52.17	52.95	91.92	38.24
	CNN Centroid + PAL (Ours)	65.99	70.59	95.22	20.81	68.27	72.76	95.06	29.57	72.07	73.55	96.93	13.10	52.90	58.48	89.90	24.75
DNANet ^[7]	CNN Full	81.96	85.90	97.54	9.11	78.06	80.50	97.72	15.71	92.70	93.37	99.05	5.77	64.80	66.94	92.59	10.04
	CNN Centroid + LESPS	55.24	61.30	90.37	19.48	57.61	63.93	91.63	6.86	60.91	63.64	91.85	33.62	41.78	50.74	84.51	11.29
	CNN Centroid + PAL (Ours)	66.97	70.63	96.28	14.66	71.01	73.33	96.96	23.05	71.79	73.67	98.94	13.35	53.83	57.71	87.21	13.42
GGL-Net ^[11]	CNN Full	82.06	85.34	97.74	12.76	78.40	79.99	96.96	20.72	92.07	92.34	99.26	4.87	66.68	67.88	93.60	17.08
	CNN Centroid + LESPS	56.66	54.79	93.55	24.41	60.06	60.45	92.02	12.14	56.34	53.24	94.92	26.52	55.39	53.89	90.57	26.06
	CNN Centroid + PAL (Ours)	67.83	70.27	95.68	16.28	72.47	73.63	95.82	26.34	70.99	72.72	98.20	13.51	58.30	58.59	87.54	15.79
UIUNet ^[9]	CNN Full	83.14	85.29	97.34	15.44	76.64	78.43	95.82	12.69	92.94	93.29	98.41	4.11	70.04	66.19	95.29	25.55
	CNN Coarse + LESPS	49.63	48.07	88.97	54.56	57.54	57.12	86.31	59.20	47.88	45.28	90.05	27.97	48.91	47.65	87.88	75.23
	CNN Coarse + PAL (Ours)	69.05	70.01	95.68	21.10	70.71	72.12	91.63	23.39	70.63	72.17	96.93	4.78	65.11	60.67	95.29	33.95
MSDA-Net ^[4]	CNN Full	83.46	85.97	97.41	17.15	74.81	78.61	95.06	30.94	93.62	94.03	99.26	9.67	70.98	67.16	93.60	19.51
	CNN Centroid + LESPS	53.57	50.34	92.43	29.05	56.98	56.00	90.87	13.24	51.72	48.17	94.18	20.27	55.94	51.48	88.22	40.67
	CNN Centroid + PAL (Ours)	69.21	72.40	97.01	15.70	70.60	72.69	96.20	26.55	74.17	75.61	98.20	9.81	58.63	61.47	93.94	17.61

results, which verifies the stability of the proposed PAL framework. Based on the results in Table 1, the batch size is uniformly set to 16 in the experiments.

2) Update period of the refined dual-update strategy.

To explore the impact of the update period of the refined dual-update strategy on the performance of the final generated model, we explore the PAL framework with different update period settings. The experimental results are shown in Table 2. Except that the update period is set to 1, the other settings have relatively stable results, which illustrates the robustness of the proposed PAL framework. The significant decrease in performance when the update period is set to 1 is because hard samples need to be trained for appropriate epochs after entering the training pool so that the model can fully learn the newly entered hard samples. It is just like when students face difficult content, they need to spend a certain amount of time to recognize, understand and apply it flexibly. If the time given is too short, students will not be able to deeply understand the knowledge, which will lead to a certain degree of knowledge confusion. In addition, the smaller the update period is set, the more time it takes to train. In the experiments, the update period is set to 5.

3) *Learning rate*. To explore the impact of the learning rate on the performance of the final generative model, we

explore the PAL framework with different learning rate settings. As shown in Table 3, the results are consistent with the relationship between the learning rate settings and performance changes in general deep learning networks. When the learning rate is set too high ($1e^{-2}$), the update step size of the model will become larger, resulting in unstable parameter updates during training, which in turn leads to training collapse. When the learning rate is set too low ($5e^{-5}$), the update step size of the model becomes smaller, which leads to slow network optimization and easy to fall into local optimality. In addition, when the learning rate is set to $5e^{-4}$ - $5e^{-3}$, the results of the final generated model are stable. This verifies the robustness of the proposed PAL framework. In the experiment, we set the learning rate uniformly to $1e^{-3}$.

4) *Missed detection rate threshold*. During this research, we discover an interesting phenomenon: there are few false detections in the detection results of single-frame infrared small target (SIRST) based on CNNs. This can also be found from the order of magnitude ($\times 10^{-6}$) of the F_a . At the same time, the falsely detected areas will be eliminated in the coarse outer updates. Therefore, we focus on exploring the threshold of the missed detection rate in the model enhancement phase. To further explore the impact of the missed detection rate threshold setting in the coarse outer

Table 6. IoU (%), nIoU (%), P_d (%) and F_a ($\times 10^{-6}$) values of different methods achieved on the separate NUAA-SIRST, NUDT-SIRST, and IRSTD-1k datasets with centroid point labels. (213:214), (663:664) and (800:201) denote the division of training samples and test samples. CNN Centroid denotes CNN-based methods under centroid point supervision.

Scheme	Description	NUAA-SIRST (213:214)				NUDT-SIRST (663:664)				IRSTD-1K (800:201)			
		IoU	nIoU	P_d	F_a	IoU	nIoU	P_d	F_a	IoU	nIoU	P_d	F_a
ACM ^[6]	CNN Full	65.67	63.74	90.11	24.01	65.33	65.12	95.87	12.92	60.45	53.70	92.26	46.06
ALCNet ^[3]	CNN Full	66.41	65.18	91.63	35.26	69.74	70.67	97.46	11.15	62.47	55.25	88.89	36.79
MLCL-Net ^[10]	CNN Full	74.68	76.50	95.82	28.74	94.03	93.97	98.73	7.72	64.86	63.35	91.25	23.23
	CNN Centroid + LESPS	32.69	32.59	82.89	20.85	34.11	32.00	89.52	46.17	46.59	45.16	86.87	29.42
	CNN Centroid + PAL (Ours)	67.64	70.28	93.92	45.00	72.67	73.87	98.31	7.79	59.14	59.21	91.25	25.79
ALCL-Net ^[2]	CNN Full	72.22	72.64	94.68	35.06	92.80	93.01	99.05	2.21	65.56	65.03	91.58	9.68
	CNN Centroid + LESPS	35.56	32.99	92.02	32.45	46.08	43.19	86.88	41.00	45.77	42.80	86.53	20.46
	CNN Centroid + PAL (Ours)	65.10	66.41	93.16	44.11	71.55	72.55	97.25	9.81	59.82	53.92	87.54	22.38
DNANet ^[7]	CNN Full	76.40	78.32	96.20	20.72	95.17	95.19	98.94	2.00	69.06	65.22	91.58	11.56
	CNN Centroid + LESPS	16.89	19.50	61.98	45.14	39.39	45.53	86.14	291.02	50.14	49.95	87.54	16.13
	CNN Centroid + PAL (Ours)	66.16	66.68	91.63	24.42	73.24	74.41	97.99	9.10	59.53	57.62	88.89	20.14
GGL-Net ^[11]	CNN Full	75.47	75.93	97.34	20.65	94.86	94.93	99.47	1.03	69.09	65.52	92.59	13.68
	CNN Centroid + LESPS	54.85	53.82	90.49	21.20	48.23	46.86	89.95	50.23	48.82	42.67	81.48	19.66
	CNN Centroid + PAL (Ours)	64.79	65.05	94.68	20.51	73.42	74.71	98.41	5.68	61.73	54.95	82.49	21.22
UIUNet ^[9]	CNN Full	78.02	76.85	96.58	14.68	95.07	95.10	98.73	0.21	70.94	64.32	91.25	10.57
	CNN Centroid + LESPS	26.05	25.27	54.75	37.52	41.60	39.43	85.93	68.23	41.40	40.42	87.88	84.93
	CNN Centroid + PAL (Ours)	66.43	69.49	96.20	14.54	74.58	75.43	98.20	4.67	61.30	55.37	91.25	36.61
MSDA-Net ^[4]	CNN Full	76.73	77.78	96.20	21.75	95.27	95.18	99.15	1.72	70.98	65.70	93.94	33.95
	CNN Centroid + LESPS	48.63	48.70	87.45	37.59	32.90	30.59	83.92	112.97	48.67	46.41	85.86	26.72
	CNN Centroid + PAL (Ours)	64.56	66.42	91.25	32.04	73.45	74.65	98.52	11.84	65.33	60.18	92.93	23.50

updates on the performance of the final generated model, we explore the PAL framework with different missed detection rate threshold settings. The experimental results are shown in Table 4. Compared with using a fixed missed detection rate threshold, using a variable value has relatively better detection results. At the same time, when the missed detection rate threshold is set larger and larger, the final performance gradually decrease. A larger threshold setting means that more harder samples will enter the training pool for training in the early of the model enhancement phase. Combined with the final results, it shows that hard samples should be input reasonably and gradually from simple to difficult in the model enhancement phase. This further verifies the effectiveness of our proposed progressive active learning idea. For the missed detection rate threshold, we set its initial threshold to 0.2 and gradually increase it to 1 as the number of epochs increases in the experiment.

D. More Quantitative Results

Considering that the main papers only conduct experiments on various datasets with coarse point labels, to further verify the effectiveness of our PAL framework, we conduct additional experiments on the SIRST3 [1], NUAA-SIRST [6], NUDT-SIRST [7] and IRSTD-1K [8] datasets with centroid point labels in this section.

Evaluation on the SIRST3 dataset with centroid point labels. As shown in Table 5, consistent with the use of

coarse point labels, when the networks (UIUNet [9], MSDA-Net [4]) with obvious performance advantages under full supervision are embedded into the LESPS framework for single point supervision tasks, the potential performance advantages of these networks cannot be effectively exploited. However, the performance change trend of each SIRST detection network equipped with our PAL framework under single-point supervision is basically consistent with that of the network under full supervision. Our PAL framework can build an efficient and stable bridge between full supervision and single point supervision tasks. Meanwhile, compared with the LESPS framework, using our PAL framework improves the IoU by 8.53%-29.10%, the nIoU by 9.33%-32.30%, and the P_d by 1.07%-6.71% on the comprehensive SIRST3-Test. The improvement is very obvious. Compared with the fully supervised task on the SIRST3-Test, our PAL framework can reach 79.33%-84.63% on IoU, 82.08%-87.05% on nIoU, and has comparable performance on P_d . In addition, by observing the results of the three decomposed test subsets, our PAL framework has a stable performance that is better than that of the LESPS framework and is in line with the full supervision performance trend. These verify that the proposed PAL framework has excellent generalizability and robustness for SIRST detection tasks in multiple scenes and multiple target types.

Evaluation on three individual datasets with centroid point labels. To further explore the stability of the PAL framework when there are few training samples and

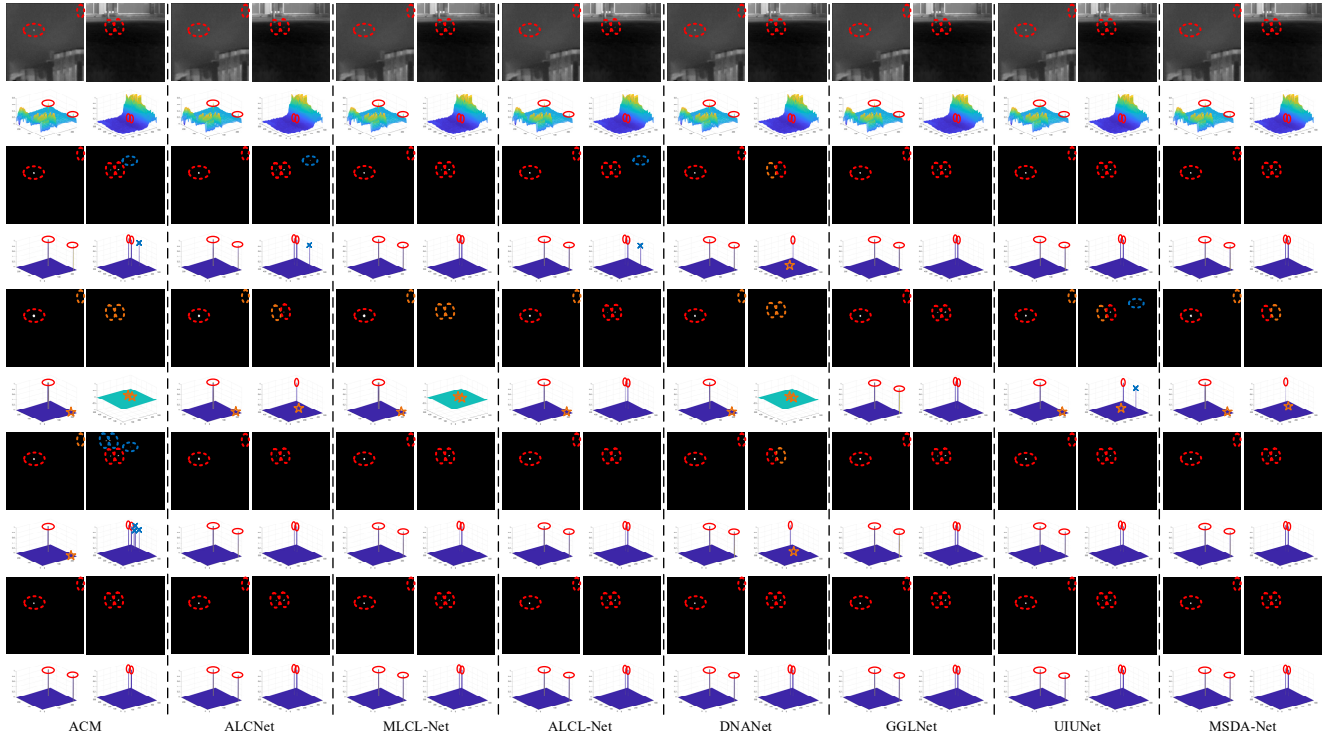


Figure 2. Visualization of several excellent methods on the SIRST3 dataset with coarse point labels. Red denotes the correct detections, blue denotes the false detections, and yellow denotes the missed detections. Every two rows from top to bottom: Image, CNN Full, CNN Coarse + LESPS, CNN Coarse + PAL, True label.

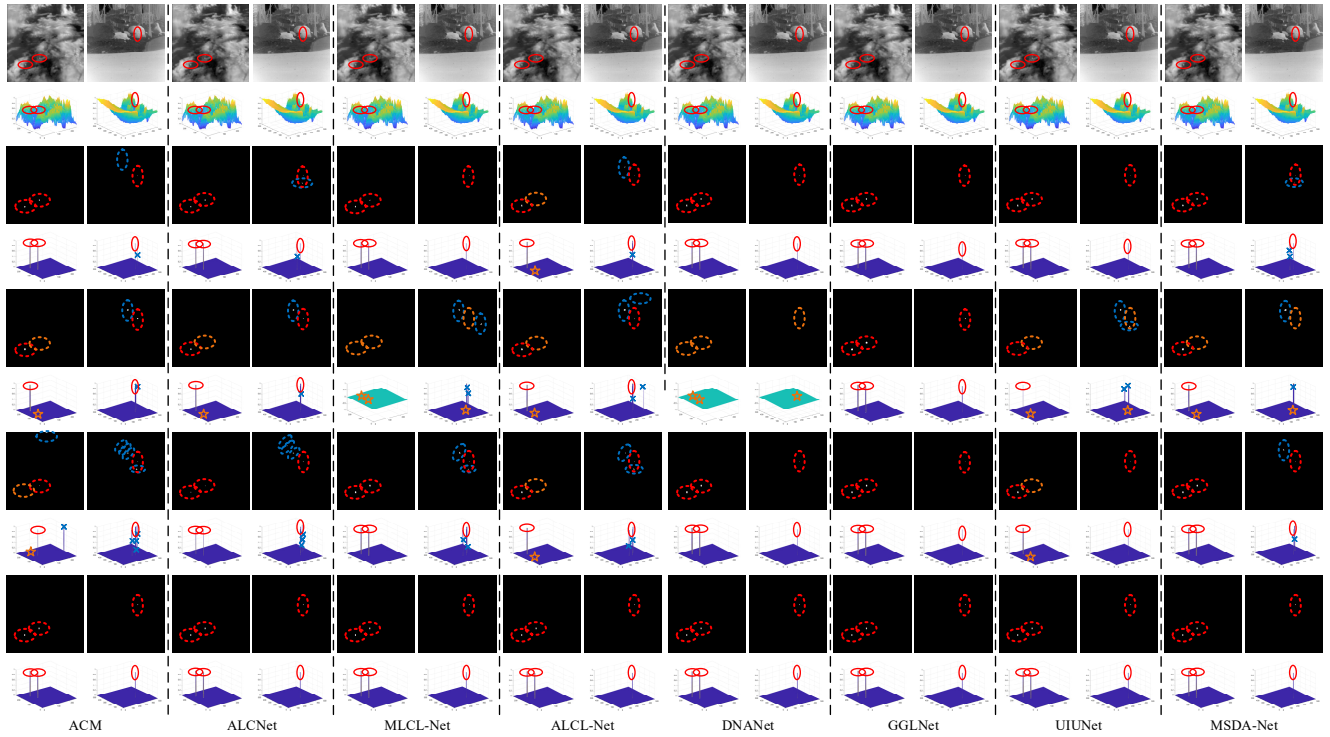


Figure 3. Visualization of several excellent methods on the SIRST3 dataset with centroid point labels. Red denotes the correct detections, blue denotes the false detections, and yellow denotes the missed detections. Every two rows from top to bottom: Image, CNN Full, CNN Centroid + LESPS, CNN Centroid + PAL, True label.

centroid point labels are used, we conduct separate experiments on the NUAA-SIRST, NUDT-SIRST, and IRSTD-1K datasets. From Table 6, consistent with the results using coarse point labels, the performance of CNNs equipped with the PAL framework is significantly better than that with the LESPS framework. At the same time, some CNNs equipped with the LESPS framework will experience the phenomenon of "model invalidity" where the final generated model does not meet the F_a requirements. Specifically, compared with the LESPS framework, using the PAL framework improves the IoU by 9.39%-49.27%, the nIoU by 7.67%-47.18%, and the P_d by 1.01%-41.45%. The improvement is very significant. In addition, except for some minor differences, the performance change trend of each SIRST detection network equipped with our PAL framework under single point supervision is basically consistent with that of the network under full supervision. These results fully verify that our PAL framework still has excellent robustness in the single point supervised SIRST detection task with a small number of training samples.

E. More Qualitative Results

To further qualitatively compare and analyze the performance of the proposed PAL framework, in this section, we present detailed visualizations of the detection results of multiple methods on multiple datasets using either coarse point labels or centroid point labels.

Visualization on the SIRST3 dataset. As shown in Fig. 2 and Fig. 3, we can find that whether using coarse point labels or centroid point labels, CNNs equipped with our PAL framework are significantly better than those equipped with the LESPS framework. From the 3D results, the LESPS framework easily leads to a large number of missed detections in difficult scenarios, whereas the PAL framework can solve this problem. In addition, for some images, the target-level detection effect of CNNs equipped with the PAL framework under single point supervision is even better than that under full supervision. From the 2D results, CNNs equipped with the PAL framework are significantly better than the LESPS framework in pixel-level segmentation. These results fully demonstrate the effectiveness of our proposed PAL framework for the SIRST detection task with single-point supervision.

Visualization on three individual datasets. As shown in Figs. 4-15, we provide a detailed visualization of various methods, different point labels and different training frameworks. First, when the LESPS framework is used, there is a significant decrease in detection performance in some networks, such as Fig. 8, Fig. 9, Fig. 14, and Fig. 15. This shows that the LESPS framework is prone to unstable performance when facing a dataset with few samples. Secondly, CNNs equipped with the PAL framework generally have more refined segmentation effects than

LESPS. Finally, compared with the detection results with full supervision, CNNs equipped with the PAL can achieve similar results with single point supervision. These results fully demonstrate the robustness of our proposed PAL framework on the single point supervised SIRST detection task with a small number of samples.

References

- [1] Xinyi Ying, Li Liu, Yingqian Wang, Ruoqing Li, Nuo Chen, Zaiping Lin, Weidong Sheng, and Shilin Zhou. Mapping Degeneration meets label evolution: Learning infrared small target detection with single point supervision. In *Proceedings of the IEEE Conference on Computer Vision and Pattern Recognition (CVPR)*, pages 15528-15538, 2023. 1, 4
- [2] Chuang Yu, Yunpeng Liu, Shuhang Wu, Xin Xia, Zhuhua Hu, Deyan Lan, and Xin Liu. Pay attention to local contrast learning networks for infrared small target detection. *IEEE Geoscience and Remote Sensing Letters*, 19: 1-5, 2022. 2, 3, 4
- [3] Yimian Dai, Yiquan Wu, Fei Zhou, and Kobus Barnard. Attentional local contrast networks for infrared small target detection. *IEEE Transactions on Geoscience and Remote Sensing*, 59(11): 9813-9824, 2021. 2, 3, 4
- [4] Jinmiao Zhao, Zelin Shi, Chuang Yu, and Yunpeng Liu. Multi-scale direction-aware network for infrared small target detection. *arXiv preprint arXiv:2406.02037*, 2024. 2, 3, 4
- [5] Jinmiao Zhao, Zelin Shi, Chuang Yu, and Yunpeng Liu. Infrared small target detection based on adjustable sensitivity strategy and multi-scale fusion. *arXiv preprint arXiv:2407.20090*, 2024. 2
- [6] Yimian Dai, Yiquan Wu, Fei Zhou, and Kobus Barnard. Asymmetric contextual modulation for infrared small target detection. In *Proceedings of the Winter Conference on Applications of Computer Vision (WACV)*, pages 950-959, 2021. 3, 4
- [7] Boyang Li, Chao Xiao, Longguang Wang, Yingqian Wang, Zaiping Lin, Miao Li, Wei An, and Yulan Guo. Dense nested attention network for infrared small target detection. *IEEE Transactions on Image Processing*, 32: 1745-1758, 2023. 3, 4
- [8] Mingjin Zhang, Rui Zhang, Yuxiang Yang, Haichen Bai, Jing Zhang, and Jie Guo. ISNet: Shape matters for infrared small target detection. In *Proceedings of the IEEE Conference on Computer Vision and Pattern Recognition (CVPR)*, pages 867-876, 2022. 4
- [9] Xin Wu, Danfeng Hong, and Jocelyn Chanussot. UIU-Net: U-Net in U-Net for infrared small object detection. *IEEE Transactions on Image Processing*, 32: 364-376, 2023. 3, 4
- [10] Chuang Yu, Yunpeng Liu, Shuhang Wu, Zhuhua Hu, Xin Xia, Deyan Lan, and Xin Liu. Infrared small target detection based on multiscale local contrast learning networks. *Infrared Physics & Technology*, 123, 2022. 3, 4
- [11] Jinmiao Zhao, Chuang Yu, Zelin Shi, Yunpeng Liu, and Yingdi Zhang. Gradient-guided learning network for infrared small target detection, *IEEE Geoscience and Remote Sensing Letters*, 20: 1-5, 2023. 3, 4

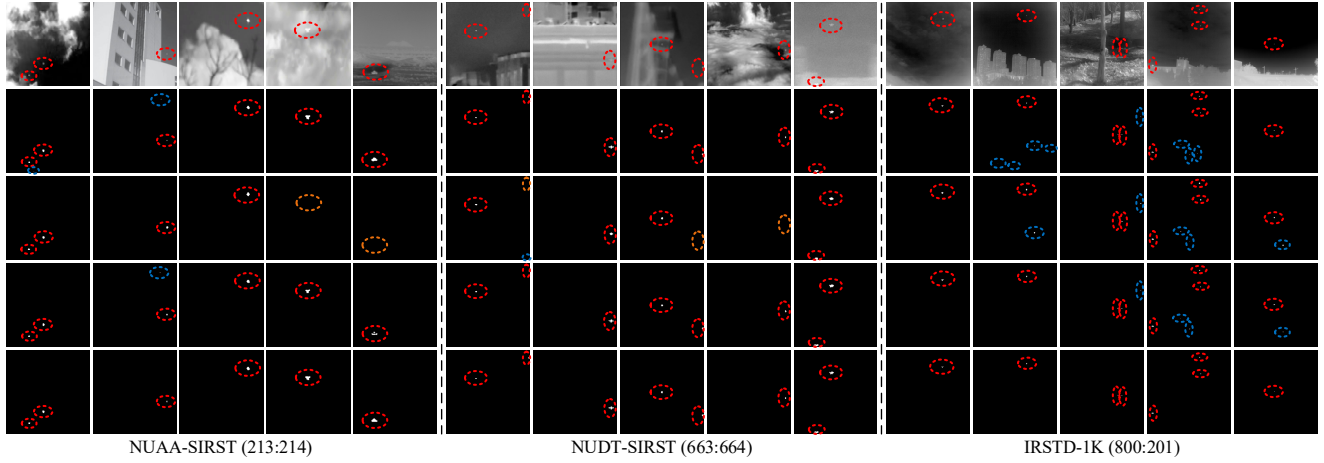


Figure 4. Visualization of MLCL-Net on the SIRST3 dataset with coarse point labels. Red, blue, and yellow denotes correct detections, false detections, and missed detections. From top to bottom: Image, CNN Full, CNN Coarse + LESPS, CNN Coarse + PAL, True label.

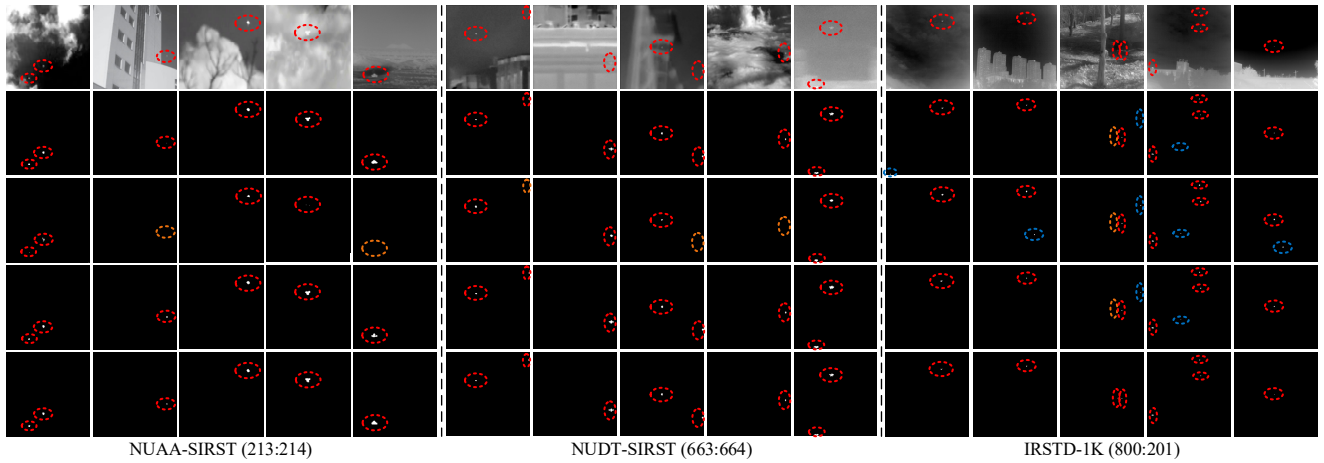


Figure 5. Visualization of ALCL-Net on the SIRST3 dataset with coarse point labels. Red, blue, and yellow denotes correct detections, false detections, and missed detections. From top to bottom: Image, CNN Full, CNN Coarse + LESPS, CNN Coarse + PAL, True label.

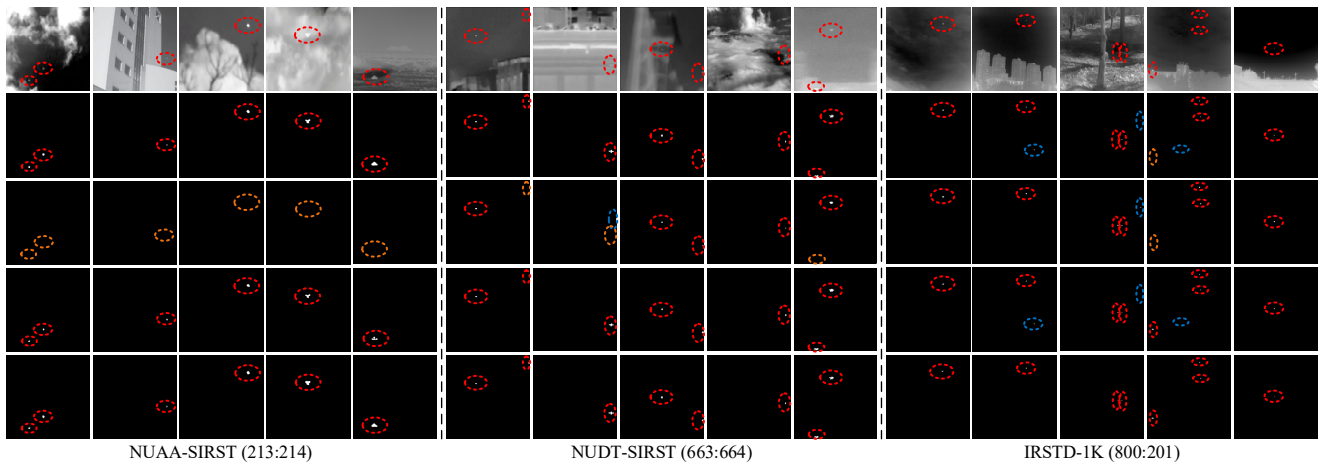


Figure 6. Visualization of DNANet on the SIRST3 dataset with coarse point labels. Red, blue, and yellow denotes correct detections, false detections, and missed detections. From top to bottom: Image, CNN Full, CNN Coarse + LESPS, CNN Coarse + PAL, True label.

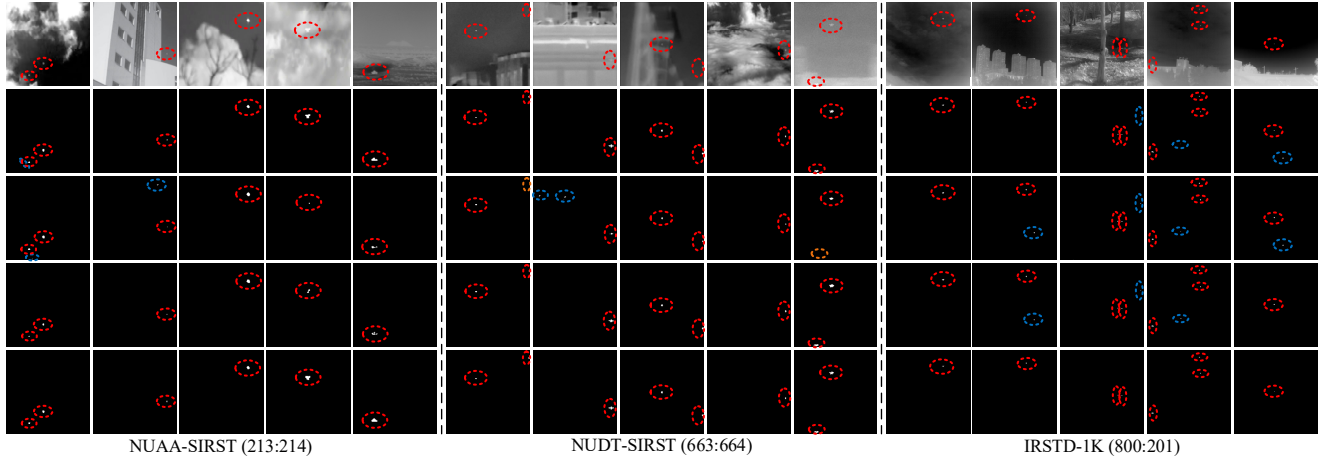


Figure 7. Visualization of GGL-Net on the SIRST3 dataset with coarse point labels. Red, blue, and yellow denotes correct detections, false detections, and missed detections. From top to bottom: Image, CNN Full, CNN Coarse + LESPS, CNN Coarse + PAL, True label.

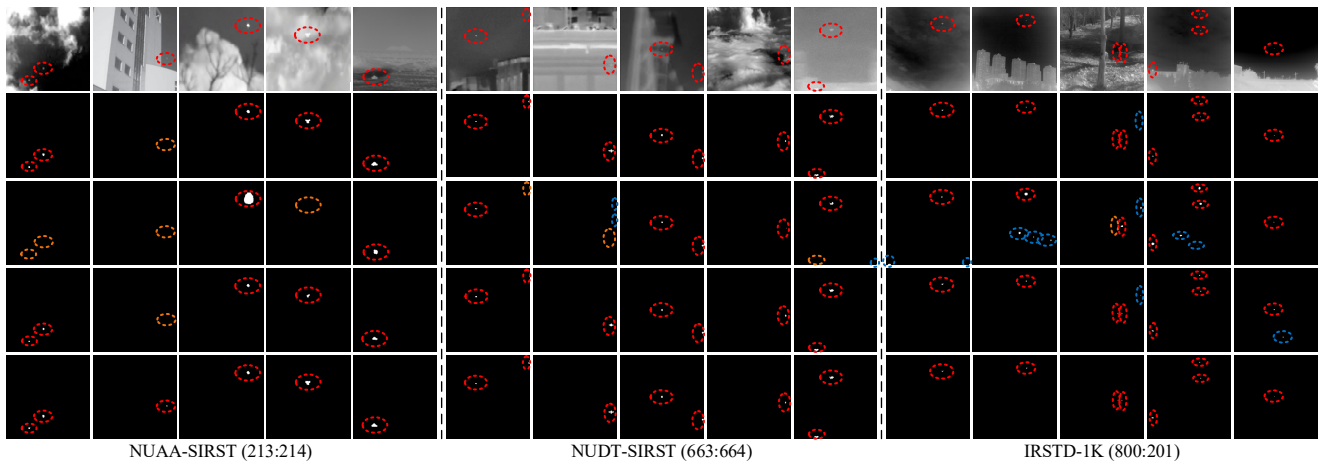


Figure 8. Visualization of UIUNet on the SIRST3 dataset with coarse point labels. Red, blue, and yellow denotes correct detections, false detections, and missed detections. From top to bottom: Image, CNN Full, CNN Coarse + LESPS, CNN Coarse + PAL, True label.

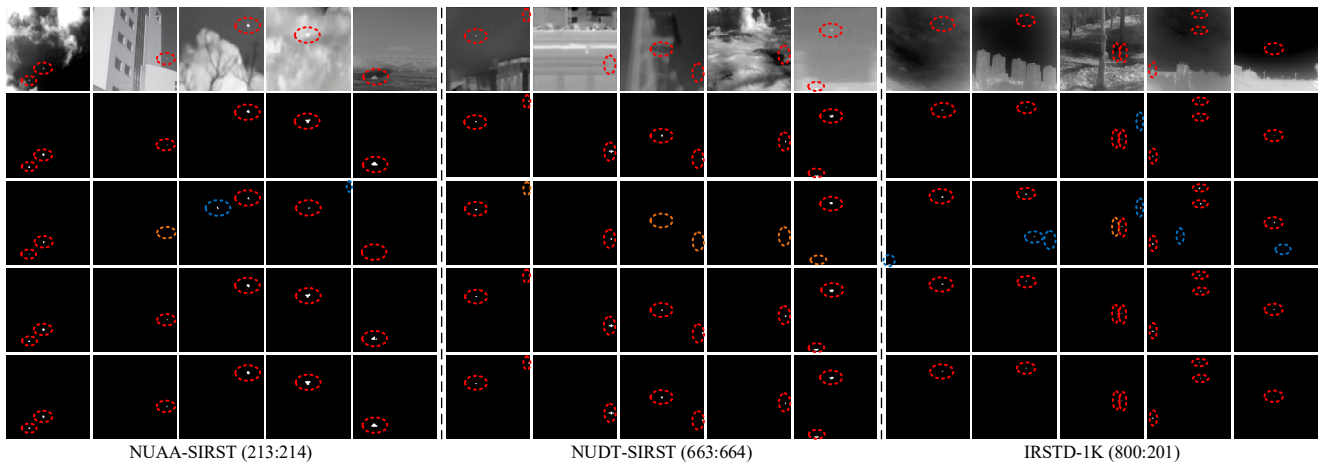


Figure 9. Visualization of MSDA-Net on the SIRST3 dataset with coarse point labels. Red, blue, and yellow denotes correct detections, false detections, and missed detections. From top to bottom: Image, CNN Full, CNN Coarse + LESPS, CNN Coarse + PAL, True label.

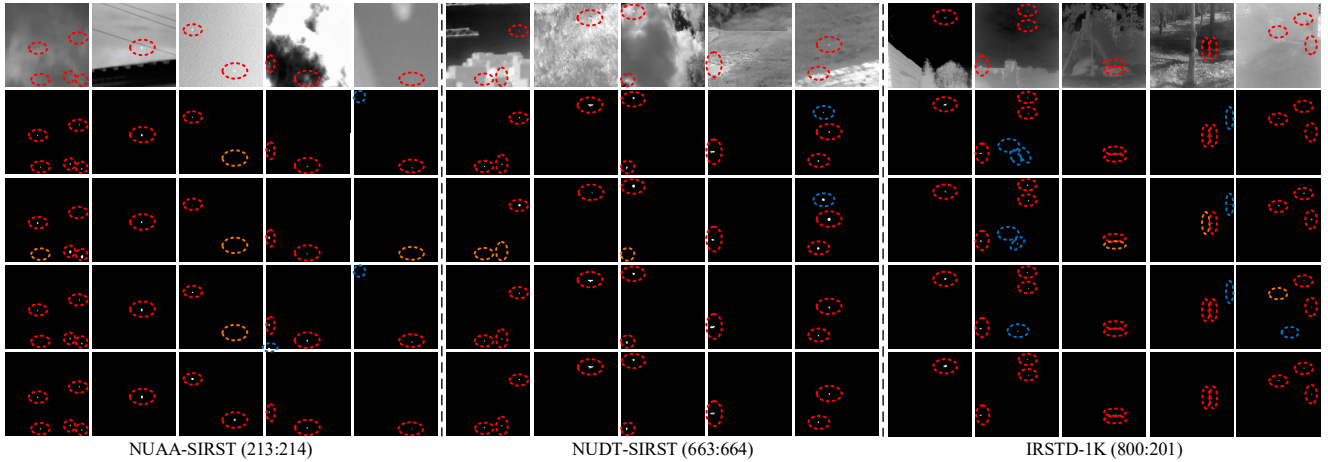


Figure 10. Visualization of MLCL-Net on the SIRST3 dataset with centroid point labels. Red, blue, and yellow denotes correct detections, false detections, and missed detections. From top to bottom: Image, CNN Full, CNN Centroid + LESPS, CNN Centroid + PAL, True label.

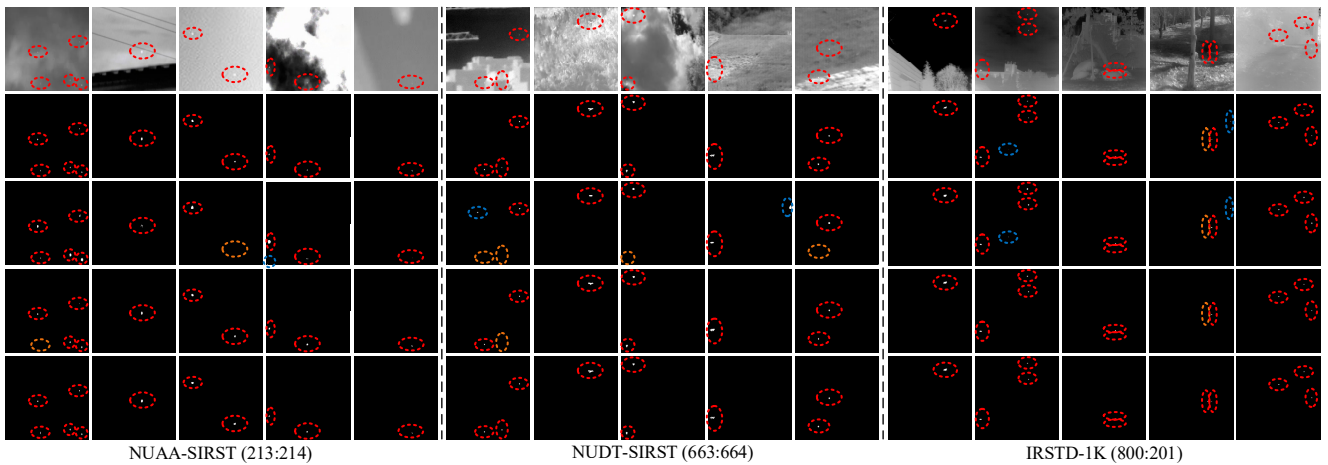


Figure 11. Visualization of ALCL-Net on the SIRST3 dataset with centroid point labels. Red, blue, and yellow denotes correct detections, false detections, and missed detections. From top to bottom: Image, CNN Full, CNN Centroid + LESPS, CNN Centroid + PAL, True label.

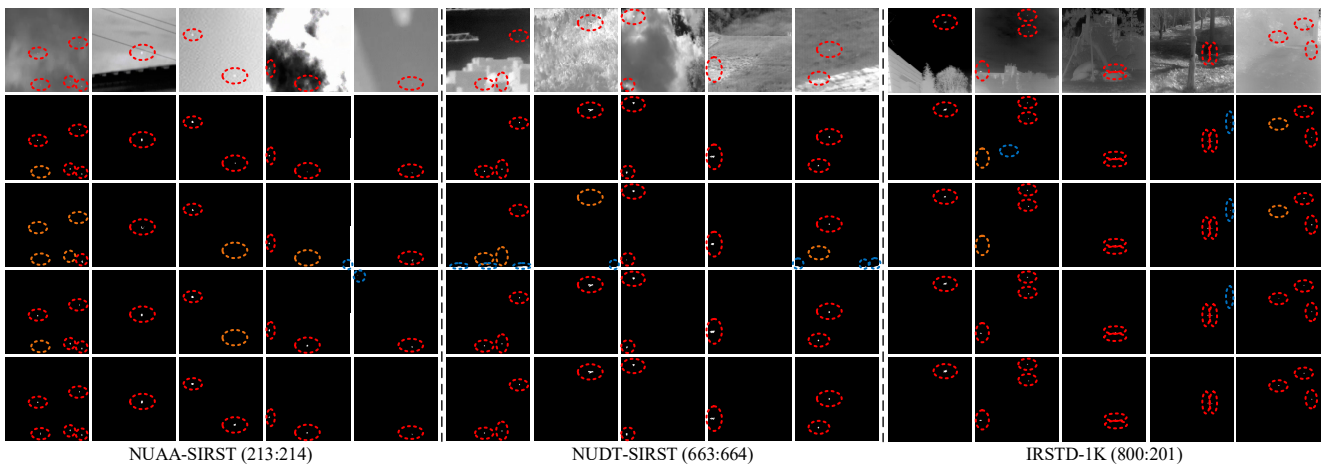


Figure 12. Visualization of DNANet on the SIRST3 dataset with centroid point labels. Red, blue, and yellow denotes correct detections, false detections, and missed detections. From top to bottom: Image, CNN Full, CNN Centroid + LESPS, CNN Centroid + PAL, True label.

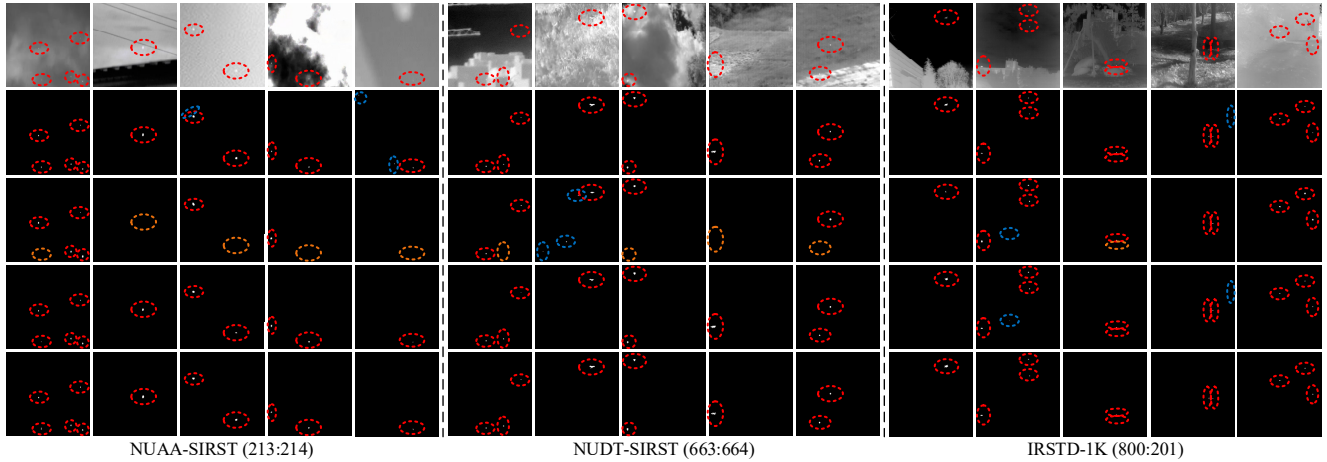


Figure 13. Visualization of GGL-Net on the SIRST3 dataset with centroid point labels. Red, blue, and yellow denotes correct detections, false detections, and missed detections. From top to bottom: Image, CNN Full, CNN Centroid + LESPS, CNN Centroid + PAL, True label.

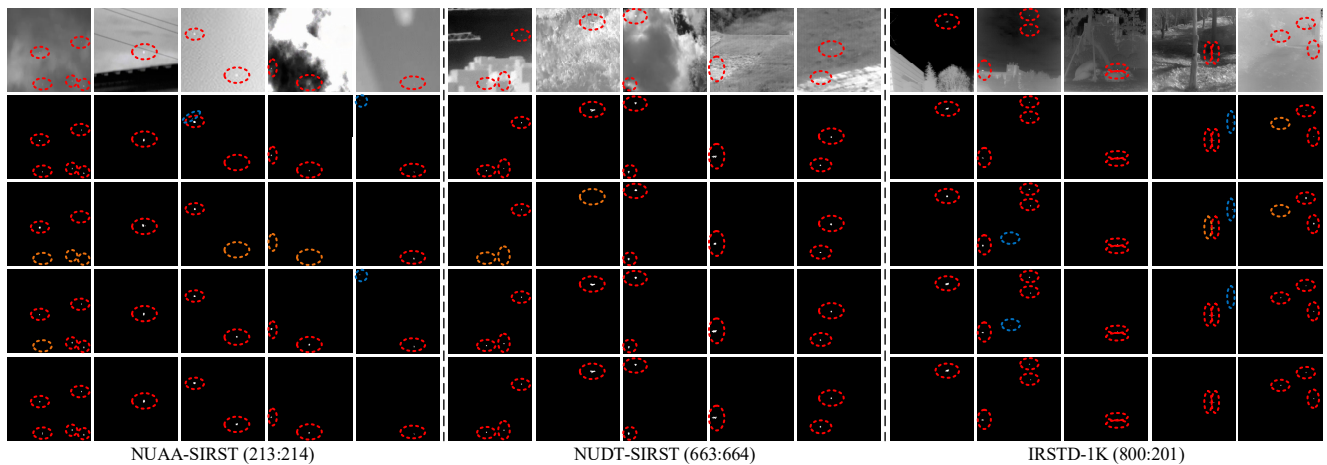


Figure 14. Visualization of UIUNet on the SIRST3 dataset with centroid point labels. Red, blue, and yellow denotes correct detections, false detections, and missed detections. From top to bottom: Image, CNN Full, CNN Centroid + LESPS, CNN Centroid + PAL, True label.

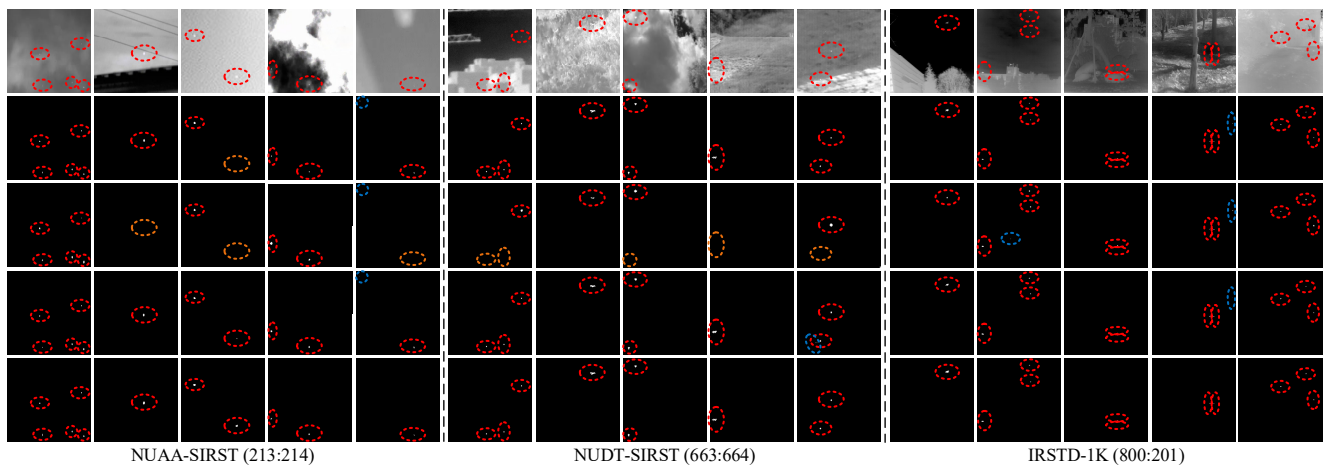


Figure 15. Visualization of MSDA-Net on the SIRST3 dataset with centroid point labels. Red, blue, and yellow denotes correct detections, false detections, and missed detections. From top to bottom: Image, CNN Full, CNN Centroid + LESPS, CNN Centroid + PAL, True label.